Application of the WRF hybrid ETKF-3DVAR data assimilation system for hurricane track forecasts

Xuguang Wang

School of Meteorology, University of Oklahoma and Center for Analysis and Prediction of Storms, Norman, OK

June 15, 2011

Revised and resubmitted to *Weather and Forecasting*

Corresponding author address:
Dr. Xuguang Wang
School of Meteorology
University of Oklahoma
120 David L. Boren Blvd.
Norman, OK, 73072
xuguang.wang@ou.edu

Abstract

A hybrid ensemble transform Kalman filter (ETKF)-three dimensional variational (3DVAR) data assimilation system developed for the WRF model was studied for the forecasts of the tracks of two major hurricanes, IKE and GUSTAV in 2008 over the Gulf of Mexico. The impact of the flow-dependent ensemble covariance generated by the ETKF was revealed by comparing the forecasts, analyses and analysis increments generated by the hybrid data assimilation method with those generated by the 3DVAR that used the static background covariance.

The root mean square errors of the track forecasts by the hybrid data assimilation (DA) method were smaller than those by the 3DVAR for both IKE and GUSTAV. Experiments showed that such improvements were due to the use of the flow-dependent covariance provided by the ETKF ensemble in the hybrid DA system. Detailed diagnostics further revealed that the increments produced by the hybrid and the 3DVAR were different for both the analyses of the hurricane itself and its environment. In particular, it was found that the hybrid, using the flow-dependent covariance that gave the hurricane-specific error covariance estimates, was able to systematically adjust the position of the hurricane during the assimilation whereas the 3DVAR was not. The study served as a pilot study to explore and understand the potential of the hybrid method for hurricane data assimilation and forecasts. Cautions need to be taken to extrapolate the results to operational forecast settings.

1. Introduction

The hybrid ensemble Kalman filter-variational data assimilation (DA) methods have been proposed (e.g., Hamill and Snyder 2000; Lorenc 2003; Etherton and Bishop 2004; Zupanski 2005; Wang et al. 2007a), implemented and tested with the real Numerical Weather Prediction (NWP) models and real data recently (e.g., Buehner 2005; Wang et al. 2008b; Buehner et al. 2010ab). Compared to a typical variational method (VAR), instead of using a static error covariance, the ensemble covariance is incorporated into the VAR framework to provide a flow-dependent estimate of the background error covariance; the ensemble is generated by a version of the ensemble Kalman filters (EnKF)[1].

Recent studies suggested that the hybrid DA systems may yield the "best of both worlds" by combining the best aspects of the variational and the EnKF systems. Studies by e.g., Wang et al. (2007b); Wang et al. (2008ab; 2009); Buehner et al. (2010ab) demonstrated that the hybrid method can improve upon a standalone VAR system because of the inclusion of the flow-dependent ensemble covariance; these studies also suggested that a hybrid system improved upon the standalone EnKF system for relatively small ensembles. In addition, a study by Campbell et al. (2009) also suggested that the hybrid system may potentially improve the utilization of observations with non-local forward operators such as the satellite radiances because the hybrid method uses the model space covariance localization rather than the observation space covariance localization. Another advantage of the hybrid system is that since the hybrid adopts the variational framework, the dynamic constraint can be conveniently added during the data assimilation. The hybrid system is also attractive for the operational NWP centers because it is built on the existing operational variational framework so that the established

[1] In the EnKF, ensemble forecasts are automatically produced and unified with the data assimilation (Hamill 2006).

capabilities in VAR (e.g., variational quality control, dynamical constraint) can be easily adopted. The above advantages of the hybrid system were also discussed in Wang (2010). Therefore several operational centers have started to develop and test the hybrid DA systems (Buehner et al. 2010; Wang 2010; D. Barker, personal communication 2010; Bishop and Hodyss 2011).

Initial tests of the hybrid DA system with real NWP models and data have shown great potential of the method (e.g., Wang et al. 2008b; Buehner et al. 2010ab). However, to the author's best knowledge, to date there are little published studies on testing the hybrid DA method for hurricane predictions, which is one of the important missions in operational NWP, especially for those countries that are prone to hurricane induced damages. While the development of a hybrid system based on the operational systems is ongoing (e.g., Wang 2010), this study served as a pilot study where we used the hybrid ETKF-3DVAR data assimilation system developed for the WRF model (Wang et al. 2008a) to explore the potential of a hybrid DA method for hurricane track forecasts. The potential was revealed by demonstrating the fundamental difference between the static and ensemble covariances during the assimilation and their impacts on the subsequent forecasts of the hurricanes.

In the hybrid ETKF-3DVAR data assimilation system for WRF, we chose to use the ETKF to generate the ensemble perturbations. In the ETKF, the ensemble perturbations were generated by solving the Kalman filter equations in the ensemble subspace without the covariance localization. Early studies (Wang and Bishop 2003; Wang et al. 2007b, 2008ab, 2009; Hacker et al. 2011) suggested that while the ETKF can generate the ensemble perturbations in a relatively less computationally expensive fashion compared to, for example, a singular vector method (Palmer et al. 1998) and an EnKF with covariance localization (e.g.,

Whitaker and Hamill 2002), it can still produce relatively skillful ensembles. In this paper we further examine if the flow-dependent ensemble covariance generated by the ETKF is a useful estimate of the background error covariance for the hurricane data assimilation, which has not been studied before.

One of the limiting factors of the hurricane track forecasts is the initial condition error associated with both the hurricanes and their environment. For the hurricane forecasts, the amount of direct in-situ observations to sample the hurricanes and their environment, especially when the hurricanes are far over the ocean, is limited. Previous studies (e.g., a hybrid DA experiment in Hamill and Snyder 2000) suggested that in such a scenario data assimilation methods using a flow-dependent ensemble covariance was more appropriate than that using a static covariance to spread the observational information to correct the background forecast. Before the emergence of the ensemble-based DA techniques such as the EnKF where flow-dependent ensemble covariance was adopted, many modeling studies adopted the vortex relocation and/or bogussing (e.g., Liu et al. 2000; Kurihara et al. 1995; Zou and Xiao 2000) techniques to initialize the hurricane forecast. While such techniques have been shown to improve the hurricane forecast, they are limited by their assumptions. How to maintain the dynamical and thermo-dynamical coherency of the hurricane and its environment while the vortex is relocated is also non-trivial and needs further studies. Several of recent studies by using the EnKF to initialize the hurricane forecasts have shown great promise (e.g., Torn and Hakim 2009; Zhang et al. 2009; Li and Liu 2009; Hamill et al. 2010). In these studies, no covariance localization or bogussing was applied. These studies further motivated this work where we explored the potential of the hybrid ETKF-3DVAR method for hurricane analyses and forecasts. Note that in the operational data assimilation system, the 3DVAR is accompanied

with the relocation technique to improve the hurricane analysis generated by the 3DVAR (Liu et al. 2000). However, since this pilot study was to understand the fundamental difference of the hybrid method and the 3DVAR for the hurricane data assimilation and forecast, we did not conduct the vortex relocation in our experiments.

This study is among the first that we are aware of that studies the hybrid ETKF-3DVAR method for the hurricane data assimilation. As an initial attempt to explore the potential of the hybrid DA method for hurricane predictions, we focus on the hurricane track forecast. A study using the hybrid data assimilation system for WRF to assimilate the radar data to examine the hurricane intensity forecast is being conducted and will be reported in a forthcoming paper (Li et al. 2011). The impacts of the flow-dependent ensemble covariance for the data assimilation and the forecast of the hurricanes were explored by comparing the forecasts and analyses generated by the hybrid method with those by the 3DVAR through the diagnostics of two major hurricanes, IKE and GUSTAV in 2008 over the Gulf of Mexico. The results of this study motivated an ongoing experiment, where we are developing and testing a hybrid data assimilation system based on the National Oceanic and Atmospheric Administration' s operational gridpoint statistical interpolation (GSI) data assimilation system for a season's hurricane forecasts. The results of this experiment with more cases will be reported in future papers. For GSI-based hybrid data assimilation algorithm, please refer to Wang (2010).

In section 2, the hybrid ETKF-3DVAR data assimilation system for WRF is briefly described. Section 3 introduces the experiment design. The results of the track analyses and forecasts for IKE and GUSTAV (2008) are presented in section 4. Section 5 provides the conclusion and discussion.

2. The Hybrid ETKF-3DVAR for WRF

The detailed description of the hybrid ETKF-3DVAR data assimilation system developed for WRF was documented in Wang et al. (2008a). As shown in Fig.1, the following four steps were repeated for each data assimilation cycle: 1) Update the ensemble mean by the hybrid ETKF-3DVAR method where the flow-dependent ensemble covariance is provided by the ensemble generated by the ETKF. 2) Update the forecast perturbations using the ETKF. 3) Add the updated ensemble perturbations in 2) to the updated ensemble mean in 1) to generate K initial ensemble members. 4) Make K forecasts starting from the K initial ensemble members forward to the next analysis time and repeat from Step 1).

One of the critical elements in the hybrid DA is the method to incorporate the ensemble covariance in the VAR framework (the thick black box in Fig. 1). In Step 1), during the variational minimization, the flow-dependent ensemble covariances were incorporated into the VAR framework by extending the control variables. For the mathematical details on this approach, please see Eqs. 1 – 5 of Wang et al. (2008a). As proved in Wang et al. (2007a), effectively, this approach is equivalent to replacing the background error covariance in a traditional 3DVAR with a weighted average of the static covariance and the ensemble covariance. The relative weights given to the ensemble covariance and the static covariance are determined by a tunable parameter $1/\beta_1$. Another tunable parameter S is also set in the system to determine the scale of the covariance localization for the ensemble covariance. The meaning of $1/\beta_1$ and S is further explained in the next section where the experiment design is described.

In the hybrid ETKF-3DVAR system, the ETKF was adopted to generate the ensemble (Wang and Bishop 2003; Wang et al. 2004, 2007b, 2008ab, 2009). In this system, the ETKF was

used to generate ensemble perturbations around the updated mean state. The ETKF updated the forecast ensemble perturbations to obtain the analysis ensemble perturbations through a transformation matrix. The transformation matrix was derived within the ensemble perturbation subspace. Assuming the covariance of the raw forecast ensemble perturbations were equal to the true forecast-error covariance, the goal of the ETKF was to choose the transformation matrix so that the outer-product of the transformed perturbations were equal to the true analysis error covariance. Eq. (9) in Wang et al. (2008a) and references therein provided the latest formula for the ETKF. There were two parameters in the ETKF that were intended to ameliorate the systematic underestimate of the analysis-error variance because of the limited ensemble size. One was an inflation factor (π) and the other was the factor (ρ) that account for the fraction of the forecast error variance projected onto the ensemble subspace. Both parameters were determined adaptively within the ETKF algorithm. Wang et al. (2007a) provided details on how to estimate these two factors adaptively for each data assimilation cycle using the innovation statistics. Table 1 lists an example of the averaged parameters π and ρ adaptively determined in one set of the IKE and GUSTAV experiments. Note that to maintain the computational efficiency, the ETKF update was performed in the low dimensional ensemble subspace and no covariance localization was applied. Therefore the ETKF alone has not been applied for data assimilation so far due to the known filter divergence problem (Hamill et al. (2001)). So far the ETKF has been mainly applied for targeting observation and for generating ensemble perturbations either for ensemble forecasting purpose or to be used in a hybrid DA system (e.g., Bishop et al. 2001, Majumdar et al. 2001; Wang et al. 2003; Wang et al. 2008ab; Hacker et al. 2011).

3. Experiment design

Experiments were performed running the version 3.1 of the WRF model (Skamarock et al. 2005), with the model domain shown in Fig. 2. The model was configured to have a 30 km horizontal grid spacing, and 35 vertical levels. The WRF physics components were WSM 5-class microphysics scheme (Hong et al. 2004), Yonsei University (YSU) boundary layer scheme (Hong et al. 2006), Kain-Fritsch cumulus parameterization scheme (Kain and Fritsch 1990), Rapid Radiative Transfer Model (RRTM) longwave scheme (Mlawer et al. 1997), and Dudhia shortwave scheme (Dudhia 1989).

Conventional in-situ data and satellite derived wind and temperature[2] available in the Global Telecommunications System (GTS) and archived in the real time at the National Center for Atmospheric Research were assimilated. Figure 3 showed a snap shot of the distribution of each type of observations. Table 2 and Fig. 4 showed the corresponding observation errors adopted. Observations were preprocessed using the observation pre-processor developed for WRF-VAR system outlined in Barker et al. (2003). Such sources of data and data processing procedures have been adopted in early published studies (e.g., Xiao et al. 2009ab). Note that dropsondes near the hurricane and in the remote environment of the hurricane that were archived in the real time were also assimilated (Figure 3e included dropsondes for IKE at 0000 UTC Sep. 7. Figure 17 showed an example of the dropsonde data for GUSTAV). For all experiments conducted, the same sets of observations were assimilated and the DA was performed every 3 hours. For the experiment using the hybrid method, a 32-member ensemble was used. As in

[2] Satellite derived data were from GOES (Geostationary Operational Environmental Satellite), METSAT (Meteorological Satellite), MODIS (Moderate Resolution Imaging Spectroradiometer), AVHRR (Advanced Very High Resolution Radiometer), NOAA polar orbiting satellites.

Wang et al. (2008b), the initial ensemble at the very beginning of the data assimilation cycles and the LBC (Lateral Boundary Condition) ensembles during the cycles were generated by adding random 32 perturbations to the NCEP Final analyses (FNL; https://dss.ucar.edu/datazone/dsszone/ds083.2). Following Torn et al. (2006), these perturbations were drawn from a normal distribution having the same covariance as the 3DVAR static background-error covariance.

Since the default 3DVAR static covariance available from the WRF release may not be the optimal model of the static background-error covariance suitable for the current data assimilation experiment, we re-calculated the static error covariances using the WRF ETKF background-forecast ensembles following the same method used by Wang et al. (2008b). Specifically, we ran the ETKF ensemble over a one-week period during the 2005 hurricane season for the same domain as shown in Fig. 2. Like the hurricane season in 2008, the hurricane season in 2005 also featured a number of hurricanes that made landfall over the US. The following steps were adopted to generate the ensemble perturbations for calculating the static covariance. The ensemble-mean background forecast was updated by the WRF 3DVAR, using the default static error covariance. The ensemble perturbations were updated by the ETKF. The updated perturbations were then added to the updated ensemble mean to generate an ensemble of analyses and started ensemble forecasts. The procedures were repeated for one week and the ensemble perturbations collected were used to calculate the static covariance following Skamarock et al. (2005). Briefly, the calculation of the static covariance was split into several stages including the calculation of the eigenvectors and eigenvalues of the vertical background errors, the calculation of the balance regression statistics and the calculation of recursive filter length scales. The above steps in calculating the static covariance has also been adopted in early

studies such as Wang et al. (2008ab) and Meng and Zhang (2008). After obtaining the newly calculated static covariance, the correlation length scale and the variance of the new static covariance were further varied by increasing and decreasing the scale and the magnitude of the variance relative to their original values. Then the 3DVAR experiments were re-run with these new static covariances. It was found that the accuracy of the track analyses of the 3DVAR experiments using the tuned static covariances were not significantly different from the default static covariances (not shown). Early studies by Wang et al. (2008b) and Meng and Zhang (2008) also found the newly generated static covariance either performed slightly better or comparable to the default static covariance for their analyses and forecasts over the continental US domain. In all of the following experiments, the newly generated static covariance was used.

As discussed earlier, as an initial attempt to reveal the potential of the hybrid method for hurricane data assimilation and prediction, the hybrid method was applied for the prediction of two major hurricanes in 2008, IKE and GUSTAV. They both reached the category 4 at their peak intensity and made the landfall at the US after passing the Gulf of Mexico. Both IKE and GUSTAV caused many deaths and extensive damage along their paths (http://www.nhc.noaa.gov/2008atlan.shtml). Table 3 gives the starting and ending dates of the data assimilation cycling periods for IKE and GUSTAV in this study. Figure 2 shows the corresponding paths from the best track data available from National Hurricane Center (http://www.nhc.noaa.gov/2008atlan.shtml).

As described in section 2, there were two tunable parameters in the hybrid method. One was the weighting factor $1/\beta_1$ which determined the weight placed on the static covariance. $1/\beta_1 = 1$ meant the full weight was placed on the static covariance and $1/\beta_1 = 0$ meant the full weight was placed on the ensemble covariance. Another parameter was the covariance

localization scale S, which determined the extent that the localization was applied on the ensemble covariance. To reveal the fundamental difference of the hybrid and the 3DVAR, in the following the results of three experiments are shown. The first experiment, denoted as HYBRID-Ens, was run with parameters $1/\beta_1 = 0$ and $S = 1500\ km$; [3]the second experiment, denoted as 3DVAR, was the traditional 3DVAR. There were two major differences among HYBRID-Ens and 3DVAR. One was that the former adopted the flow-dependent ensemble covariance as the background covariance whereas the 3DVAR adopted the static covariance. The second was that the former as other ensemble-based data assimilation methods used the mean or average of the ensemble forecasts as the background forecast whereas the 3DVAR used a single deterministic forecast as the background forecast. To isolate the impacts of these two differences on the performance of the 3DVAR and the HYBRID-Ens, we included the third experiment, denoted as HYBRID-Static. The only difference between the HYBRID-Static and the 3DVAR was that in the former the ensemble mean was used as the background whereas 3DVAR used the single deterministic forecast as the background. The experiment HYBRID-Static was conducted by simply setting $1/\beta_1 = 1$. If the HYBRID-Static and the 3DVAR were similar to each other and were both different from the HYBRID-Ens, then it was the flow-dependent ensemble covariance that made the difference between the HYBRID-Ens and the 3DVAR. Besides the above 3 experiments, we also tried several experiments with different combinations of S and $1/\beta_1$ such as $1/\beta_1 = 0, 0.5, 1$ and $S = 250, 500, 1000, 1500$ km. Our evaluation showed that the performances of these experiments did not significantly improve

[3] Note that a hybrid method means a hybrid of the variational and ensemble Kalman filter frameworks. The weighted average of the static covariance and the ensemble covariance where the weights on the static and ensemble covariance are non-zero is not essential for a hybrid method. Section 1 describes other advantages of the hybrid of the two frameworks in addition to the flexibility of varying the weights on the static and ensemble covariances.

upon the experiment HYBRID-Ens. Therefore we focus on the comparison of the HYBRID-Ens with the 3DVAR in this paper.

As mentioned in section 2, there were two parameters inherent in the ETKF, the inflation factor and the fraction factor. The inflation factor defined the amount of inflation needed in order to make the spread of the ensemble to be consistent with the forecast errors on average. The fraction factor defined the percentage of the forecast error variance explained by the ensemble subspace. Both were estimated adaptively in the space of observed variables in the ETKF. For details please refer to Wang et al. (2007b). Table 1 showed the averaged inflation factor and fraction factor adaptively determined in the HYBRID-Ens experiments for both IKE and GUSTAV. On average, for the HYBRID-Ens experiments, an inflation factor of 6.70 and 7.22 were used for IKE and GUSTAV respectively. Since covariance localization was not used in the ETKF, the inflation factor for the ETKF was in general larger than that typically used by the EnKF with covariance localization. A fraction factor of 39.96% and 38.94%, which meant the ensemble subspace[4] explained 39.96% and 38.94% of the total 3-hour forecast error variance in the observation space, were used for IKE and GUSTAV respectively. Since the inflation factor and the fraction factor were determined adaptively, their values reflected the quality of the ensemble in representing the forecast errors. The magnitudes of the inflation factor and the fraction factor depend on the configuration of the ensemble (e.g. the ensemble size), the observation network and the dynamics of the system being forecasted. Examples of such factors in other applications can be found in Wang et al. (2007b, 2008ab, 2009). In the current real observation experiments, the inflation factor accounted not only for the ETKF's systematic

[4] The dimension of the ensemble subspace is the number of ensemble members minus 1, which was 31 in the current study. This dimension was smaller than the number of degrees of freedom of the forecast errors. Therefore only a fraction of the forecast errors were projected or explained by the ensemble subspace (Wang et al.2007b).

underestimation of the error variance owing to the limited ensemble size, but also for other misrepresented error sources such as errors from the model.

To evaluate the skill of the track forecasts, we initialized deterministic forecasts using the analyses generated by different DA methods. The forecasts were initialized every 12 hours during the data assimilation cycles. The statistics of the track forecast errors were collected by using these forecasts initialized after two days' data assimilation cycles. The root mean square (RMS) track forecast errors up to 72 hour forecast lead times were calculated by comparing the forecast against the best track data. A two-day spin-up period was adopted following Torn (2011) so that the ensemble had little memory of the initial randomly generated ensemble.

4. Results

In this section, we evaluate the skill of the track analyses and forecasts by the HYBRID-Ens, HYBRID-Static and 3DVAR experiments. Diagnostics were conducted to understand how the differences in the analyses could contribute to the difference in the forecasts and how different the analyses increments were in different experiments. The goal of such diagnostics was to facilitate the understanding of the differences among the data assimilation schemes and how such differences contributed to the difference in their performances. The results for IKE and GUSTAV are presented in subsections 4a and 4b respectively.

a. Results for IKE

Figure 5 and Figure 6 show respectively the analyzed tracks and the absolute errors of the analyzed tracks for IKE every 6 hours by the 3DVAR, HYBRID-Static, and HYBRID-Ens. The analyzed tracks by the three experiments all aligned with the best track data in general. The root-

mean square errors of the track forecasts (Fig. 7) showed that the track forecasts by the HYBRID-Ens on average were more accurate than both the 3DVAR and the HYBRID-Static especially for the forecast lead times longer than 2 days. Figure 7 also show that the accuracy of the track forecasts by the HYBRID-Static was similar to that of the 3DVAR. These results suggested that the improvement of the HYBRID-Ens forecast relative to the 3DVAR was mainly because of the use of the flow-dependent ensemble covariance as opposed to a static covariance to estimate the background error covariance, rather than the use of the ensemble averaging in place of a single forecast as the background forecast. Further examining the forecasts where the 3DVAR was significantly worse than the HYBRID-Ens, we found that the 3DVAR track forecasts had significant westward bias whereas the HYBRID-Ens track forecast aligned with the best track data much better. Figure 8 showed an example of such forecasts initialized with the analyses at 0000 UTC 9 Sep. 2008. Note that many of the operational forecasts in the National Hurricane Center also showed a westward bias over the western Gulf of Mexico several days before the landfall (http://www.nhc.noaa.gov/pdf/TCR-AL092008_Ike_3May10.pdf). The WRF forecast initialized by the analyses of the operational Global Forecast System model (GFS) was similarly biased toward the west and was shown in Fig. 8 as a reference.

What were the differences of the analyses at 0000 UTC 9 Sep. 2008 generated by the different DA methods that contributed to their differences in the track forecasts of IKE? Since the accuracy of the hurricane track forecasts depended both on the analysis of the hurricane itself and the environment that the hurricane was embedded in, analyses for both the hurricane itself and its environment were examined. Figure 9 showed the 500 hPa geopotential height analyses at 0000 UTC 9 Sep. 2008 by the HYBRID-Ens and the 3DVAR. IKE was embedded in the southwest periphery of the subtropical high. The subtropical high in the 3DVAR analysis

extended more to the south in the southwest quadrant of Gulf of Mexico than that in the HYBRID-Ens. This difference in the 3DVAR and the HYBRID-Ens analyses suggested that in IKE's environment analyzed by the 3DVAR there was a stronger easterly. This stronger easterly could contribute to the westward bias in the subsequent forecast of the 3DVAR. To further confirm this hypothesis, following Chan and Gray (1982) we calculated the averaged hurricane environmental wind 5-7° from the center of the hurricane at 500 hPa. It was found that the easterly wind around IKE in the 3DVAR was 1.23 ms^{-1} stronger than that in the HYBRID-Ens. Figure 10 show the forecast of the 500 hPa geopotential height at the 48 hour lead time. The westward bias of the track forecast by the 3DVAR was associated with a stronger subtropical high forecast compared to the HYBRID-Ens. Consistently, a recent study by Brennan and Majumdar (2011) examining the track forecast errors from the operational model also hypothesized the westward bias was because the ridge to the north of IKE was too strong. In addition to the differences in the analyzed environment, IKE itself was also analyzed differently by the 3DVAR and the HYBRID-Ens. Figure 11 showed the vertical cross-section of the wind speed of IKE in the 3DVAR and HYBRID-Ens analyses at 0000 UTC 9 Sep. 2008. The IKE analyzed by the 3DVAR was smaller in size and less intense than that by the HYBRID-Ens, which was further confirmed by examining the sea level pressure and the vertical cross-section of the relative vorticity (not shown). This difference in size and intensity led to a weaker beta drift in the 3DVAR than the HYBRID-Ens (Smith 1993), which could also contribute to the relative westward track forecast by the 3DVAR as compared to the HYBRID-Ens.

To further understand why the analyses at 0000 UTC 9 Sep. 2008 by the 3DVAR and the HYBRID-Ens were different, we examined the analysis increments before reaching this time. The increments of the 3DVAR and the HYBRID-Ens were different for both the hurricane and

its large scale environment. Figure 12 show a representative example at 0000 UTC 8 Sep. 2008 for the 500 hPa geopotential height. For the HYBRID-Ens, the absolute increment for IKE was larger than that for the environment (Fig. 12b) whereas for the 3DVAR, the absolute increment for IKE was less or comparable to the increment for the environment (Fig. 12a). Figure 12c show the spread of the background ensemble of the 500 hPa geopotential height in the HYBRID-Ens. The spread suggested the ETKF-estimated forecast uncertainty was larger around IKE than its environment, which was consistent with the larger increment around IKE than its environment in the HYBRID-Ens (Fig. 12b). For the 3DVAR, the increment for the environment featured an increase of the geopotential height between the Yucatan Peninsula and the Cuba Island and a decrease of the height along Florida, Cuba and Jamaica. The increment for IKE itself was also different between the 3DVAR and the HYBRID-Ens. The increment for IKE by the 3DVAR was much weaker compared to that by the HYBRID-Ens. The increment by the HYBRID-Ens showed a dipole pattern. This increment pattern suggested that the HYBRID-Ens used observations to correct the position of IKE in the background forecast by moving it to the southeast of the forecasted position. This result suggested that the HYBRID-Ens using the flow-dependent ensemble covariance naturally and systematically corrected the position of the hurricane without using the extra vortex relocation procedure often used by the operational 3DVAR system. Note that here flow-dependent meant the ensemble covariance provided an estimate of the uncertainty of the position of the hurricane. In other words, the hybrid provided a hurricane-specific background error covariance.

b. Results for GUSTAV

Figure 13 and Figure 14 show respectively the analyzed tracks and the absolute errors of the analyzed tracks for GUSTAV every 6 hours by the 3DVAR, HYBRID-Static, and HYBRID-

Ens. Tracks analyzed by both the 3DVAR and the HYBRID-Static drifted to the southwest relative to the best track data starting from 0000 UTC 29 Aug. 2008. The most deviate of the 3DVAR and the HYBRID-Static analyses from the best track occur at 0000 UTC 30 Aug. 2008, after which GUSTAV analyzed by the 3DVAR and the HYBRID-Static started to turn to the north and caught the best track around 1200 UTC 31 Aug. 2008. While the tracks analyzed by the 3DVAR and the HYBRID-Static made a spurious loop, the track analyzed by the HYBRID-Ens followed the best track more closely.

The root-mean square errors of the track forecasts (Fig. 15) showed that the track forecast by the HYBRID-Ens was more accurate than both the 3DVAR and the HYBRID-Static with the former gaining 1-2 day lead time relative to the latter two. The accuracy of the track forecast by the HYBRID-Static was similar to that by the 3DVAR. As in the IKE case, these results also suggested that the improvement by the HYBRID-Ens relative to the 3DVAR was mainly because of the use of the flow-dependent ensemble covariance in the HYBRID-Ens. Further examining those forecasts, we found that forecasts initialized during 0000 UTC 29 Aug. 2008 ~ 1200 UTC 31 Aug. 2008 using the analyses generated by the 3DVAR was significantly worse than those by the HYBRID-Ens. Note that as shown in Fig. 13 and Fig. 14, during this period of time, the track analyzed by the 3DVAR was less accurate than that by the HYBRID-Ens, which contributed to the worse subsequent forecasts of the 3DVAR. Therefore, in the next we show what could contribute to the worse analyses by the 3DVAR during this time period, 0000 UTC 29 Aug. 2008 ~ 1200 UTC 31 Aug. 2008.

Figure 16 show the 500 hPa geopotential height analysis at 0000 UTC 29 Aug. 2008. GUSTAV was positioned in the southeast quadrant of a high pressure system over Gulf of Mexico. This high pressure system was stronger in the 3DVAR analysis than in the HYBRID-

Ens analysis. Therefore in the 3DVAR analysis, GUSTAV's environment had a stronger north-easterly wind, which was verified by calculating the environmental wind 5-7° from the center following Chan and Gray (1982). It was found that the easterly (northerly) wind around GUSTAV in the 3DVAR was 1.03 ms^{-1} (1.03 ms^{-1}) stronger than the HYBRID-Ens. The same was found at 1200 UTC 29 Aug. 2008 at which time relative to the HYBRID-Ens, the 3DVAR had a 2.36 ms^{-1} (1.67 ms^{-1}) easterly (northerly) environmental wind anomaly around GUSTAV. The stronger high pressure system in the 3DVAR seen at 0000 UTC 29 therefore contributed to the subsequent southwest drift of the track starting from 0000 UTC 29 Aug. 2008.

While dropsondes data were available before 0000 UTC 29 in the archive, these dropsondes were mostly in the vicinity of GUSTAV rather than its remote environment such as the Gulf of Mexico (Fig. 17a). Therefore the 3DVAR, with a static covariance, could not use these dropsondes to directly correct the environment over the Gulf of Mexico where a stronger high pressure system was seen at 0000 UTC 29 (Fig. 16). During the period of 0000 UTC 29 ~ 0000 UTC 30 Aug. 2008 when the 3DVAR analyzed GUSTAV gradually deviated from the best track, the 3DVAR using a static covariance could not systematically adjust the position of GUSTAV as what a flow-dependent covariance was capable of doing (e.g., the dipole increment for the hurricane seen in the HYBRID-Ens) . Previous studies (e.g., Hamill and Snyder 2000) suggested that given the nature of the static covariance, in order to correctly adjust the position of the hurricane during the assimilation, a large amount of data that directly sample the hurricane were needed. Note that during the time period when the analyzed GUSTAV started to drift (0000 UTC 29 ~ 1800 UTC 29 Aug. 2008), the number of dropsondes in the vicinity of GUSTAV that were available from the real-time data archive used was relatively small (Fig. 17b). Also as shown in Fig. 17b, by the time of the dropsondes, GUSTAV estimated in the

3DVAR background forecasts already drifted away from the best track. Therefore, assimilating these limited dropsondes using the static covariance could not bring the drifted GUSTAV back to the right locations. This result was consistent with early studies such as Hamill and Snyder (2000) where static covariance was shown to be particularly poorer than the flow-dependent covariance in the data sparse region. In the data archive, dropsondes that sampled the Gulf of Mexico started to be available at 1800 UTC 29, by which time GUSTAV analyzed by the 3DVAR already drifted away from the best track.

At 0000 UTC 30 Aug. 2008, the 3DVAR analyzed GUSTAV reached its southern-most point of the analyzed track (Fig.13). During the period of 0000 UTC 30 ~ 1200 UTC 31 Aug. 2008, 3DVAR assimilated observations which sampled GUSTAV and formed spurious double vortices (e.g., Fig. 18a). While the increments by the 3DVAR further enhanced the double vortices, the dipole pattern increments of the HYBRID-Ens again showed the systematic adjustment of the position of the hurricane as in the IKE case (Fig. 18b).

As mentioned in section 1, the vortex relocation technique is used in the operational data assimilation system to further improve the hurricane analyses by the operational 3DVAR (Liu et al. (2000)). If accompanying the 3DVAR experiment with a procedure like the vortex relocation, the erroneous behavior of the analyzed track such as the drift of the vortex and the double vortices in the 3DVAR experiment could be reduced. The results of the hybrid on the other hand suggested that adopting the flow-dependent ensemble covariance can correct the location of the hurricane systematically without using the vortex relocation procedure or bogussing. As also discussed in section 1, vortex relocation relied on several assumptions and further work was still needed to maintain the dynamical and thermo-dynamical coherency of the hurricane and its environment while the hurricane was relocated (Liu et al. 2000).

5. Conclusion and discussion

A hybrid ETKF-3DVAR data assimilation (DA) system developed for WRF was applied to explore the potential of a hybrid ensemble-variational data assimilation method for the hurricane track forecasts. The impact of the flow-dependent ensemble covariance was revealed by comparing the forecasts, analyses and analyses increments generated by the hybrid DA method with those generated by the 3DVAR that used the static background error covariance. Two major hurricanes, IKE and GUSTAV in 2008 over the Gulf of Mexico were considered in this study.

The root mean square errors of the track forecasts initialized by the analyses generated by the hybrid DA method were smaller than those by the 3DVAR for both IKE and GUSTAV with the hybrid method gaining 1~2 day lead time. Such improvement was shown due to the flow-dependent ETKF ensemble covariance used in the hybrid DA method as opposed to a static covariance typically used in the 3DVAR. Such conclusion was consistent with early studies of comparing the ensemble based DA methods with the 3DVAR for other applications (e.g., Wang et al. 2008ab; Meng and Zhang 2008; Whitaker et al. 2008; Buehner et al. 2010b). Detailed diagnostics further revealed that the increments produced by the hybrid and the 3DVAR were different for both the analyses of the hurricane itself and the environment of the hurricane. In particular, it was found that the hybrid using the flow-dependent ensemble covariance was able to systematically adjust the position of the hurricane during the assimilation whereas the 3DVAR was not.

The current study served as a pilot study to examine the potential of a hybrid DA system for hurricane forecasts and to understand the fundamental differences of the flow-dependent ensemble covariance versus a static covariance for hurricane forecasts. Cautions need to be taken to extrapolate the results to the operational system. First no satellite radiance data were assimilated and not all hurricane surveillance observations were in the data archive. Second, the operational 3DVAR system is accompanied by a vortex relocation technique (Liu et al. 2000), which was not applied in the current study. We also examined and conducted diagnostics for only two major hurricanes. Further experiments with more cases and assimilating more complete observations are needed to assess the generality of the results. Results from experiments with a season's cases using the hybrid data assimilation system being developed based on NOAA operational 3DVAR data assimilation system assimilating all operational data including direct assimilation of satellite radiance data will be reported in future papers. The impact of conducting the vortex relocation will also be examined in such experiment. Besides the track forecasts, experiments using the WRF hybrid data assimilation system to assimilate radar data to explore the potential of the hybrid data assimilation system for the hurricane intensity forecasts are also ongoing and will be reported in future papers (Li et al. 2011).

In addition, as an initial effort to understand the potential of the hybrid DA system for the hurricane forecasts, we compared it with the 3DVAR. We also recommend direct and thorough comparisons with other data assimilation techniques such as the EnKF and the 4DVAR so as to understand the relative advantages and disadvantages of different techniques in hurricane forecasts. The hypothesis of the advantages of the hybrid system relative to a standalone EnKF and VAR methods as discussed in section 1should be further explored in the context of the hurricane forecasts.

Work is still needed to further improve the hybrid system by improving covariance localization method such as the scale-dependent/aware covariance localization, by applying the ETKF over local region to reduce the impact of sampling error in the ETKF update (Bowler et al. (2009)) and by using more sophisticated ways to represent model errors in the ensemble.

Acknowledgements. The author was supported by University of Oklahoma faculty start up award 122-792100, NOAA THORPEX funds NA08OAR4320904 and NASA New Investigator Program Award NNX10AQ78G. The experiments were conducted on the supercomputers hosted by the Supercomputing Center for Education and Research at University of Oklahoma.

References

Barker, D., W. Huang, Y. Guo, A. Bourgeois, 2003: A three dimensional variational data assimilation system for use with MM5. NCAR Tech. Note 453+STR, National Center for Atmospheric Research, Boulder, CO, 68 pp.

Bishop, C. H., and D. Hodyss, 2011: Adaptive Ensemble Covariance Localization in Ensemble 4D-VAR State Estimation. *Mon. Wea. Rev*., **139**, 1241-1255.

Bowler, N. E., A. Arribas, S. E. Beare, K. R. Mylne, and G. J. Shutts, 2009: The local ETKF and SKEB: Upgrades to the MOGREPS short-range ensemble prediction system. *Q. J. R. Meteorol. Soc.* 135: 767–776 (2009)

Buehner, M., 2005: Ensemble-derived stationary and flow-dependent background-error covariances: evaluation in a quasi-operational NWP setting. *Quart. J. Roy. Meteor. Soc.*, **131**, 1013-1043.

−, P. L. Houtekamer, C. Charette, H. L. Mitchell, and B. He, 2010: Intercomparison of Variational Data Assimilation and the Ensemble Kalman Filter for Global Deterministic NWP. Part I: Description and Single-Observation Experiments. *Mon. Wea. Rev.*, **138**, 1550-1566.

−, P. L. Houtekamer, C. Charette, H. L. Mitchell, and B. He, 2010: Intercomparison of Variational Data Assimilation and the Ensemble Kalman Filter for Global Deterministic NWP. Part II: One-Month Experiments with Real Observations. *Mon. Wea. Rev.*, **138**, 1567-1586.

Campbell, W. F., C. H. Bishop, and. D. Hodyss, 2009: Vertical covariance localization for satellite radiances in ensemble Kalman filters. *Mon. Wea. Rev.*, in press.

Chan, J. C. L., and W. M. Gray, 1982: Tropical cyclone movement and surrounding flow relationships. *Mon. Wea. Rev.*, **110**, 1354-1374.

Dudhia, J., 1989: Numerical study of convection observed during the winter monsoon experiment using a mesoscale two-dimensional model. J. Atmos. Sci., 46, 3077–3107.

Etherton, B., and C. H. Bishop: Resilience of Hybrid Ensemble/3DVAR Analysis Schemes to Model Error and Ensemble Covariance Error. *Mon. Wea. Rev*., **132**, 1065-1080.

Hacker, J. P., S.-Y. Ha, C. Snyder, J. Berner, F. A. Eckel, E. Kuchera, M. Pocernich, S. Rugg, J. Schramm, and X. Wang, 2010: The U.S. Air Force Weather Agency's mesoscale ensemble: Scientific description and performance results. *Tellus*, in press.

Hamill, T. M., and C. Snyder, 2000: A hybrid ensemble Kalman filter-3D variational analysis scheme. *Mon. Wea. Rev.*, **128**, 2905-2919.

−, J. S. Whitaker and C. Snyder, 2001: Distance-Dependent Filtering of Background Error Covariance Estimates in an Ensemble Kalman Filter. *Mon. Wea. Rev*., **129**, 2776-2790.

−, 2006: Ensemble based atmospheric data assimilation. *Predictability of Weather and Climate,* R. Hagedorn and T. N. Palmer, Eds., Cambridge Press, 124–156.

−, J. S. Whitaker, M. Fiorino, and S. J. Benjamin, 2010: Global ensemble predictions of 2009's tropical cyclones initialized with an ensemble Kalman filter. Mon. Wea. Rev., in press.

Hong, S. Y., J. Dudhia, and S. H. Chen, 2004: A revised approach to ice microphysical processes for the bulk parameterization of clouds and precipitation. Mon. Wea. Rev., 132, 103–120.

Hong, S.-Y., Y. Noh, and J. Dudhia, 2006: A new vertical diffusion package with an explicit treatment of entrainment processes. Mon. Wea. Rev., 134, 2318–2341.

Kain, J. S. and J. M. Fritsch, 1990: A one-dimensional entraining detraining plume model and its application in convective parameterization. J. Atmos. Sci., 47, 2784–2802.

Kurihara, Y. M., A. Bender, R. E. Tuleya, and R. J. Ross, 1995: Improvements in the GFDL hurricane prediction system. Mon. Wea. Rev., 123, 2791–2801.

Li, J. and H. Liu, 2009: Improved hurricane track and intensity forecast using single field of-view Advanced IR Sounding measurements. *Geophys. Res. Lett*., 36, L11 813.

Li, Y., X. Wang and M. Xue, 2011: Assimilation of Radar Radial Velocity Data with the WRF Ensemble-3DVAR Hybrid System for the Prediction of Hurricane IKE (2008). Paper 542, *15th Symposium on Integrated Observing and Assimilation Systems for the Atmosphere, Oceans and Land Surface*, Seattle, WA, Amer. Meteor. Soc.

Liu, Q., T. Marchok, H.-L. Pan, M. Bender, and S. J. Lord, 2000: Improvements in hurricane initialization and forecasting at NCEP with global and regional (GFDL) models. Tech. rep., NOAA Tech. Procedures Bull. 472, 7 pp. pp., Camp Springs, MD.

Lorenc, A. C. 2003: The potential of the ensemble Kalman filter for NWP – a comparison with 4D-VAR. *Quart. J. Roy. Meteor. Soc.*, **129**, 3183-3203.

Mlawer, E. J., S. J. Taubman, P. D. Brown, M. J. Iacono, and S. A. Clough, 1997: Radiative transfer for inhomogeneous atmosphere: RRTM, a validated correlated-k model for the long-wave. J. Geophys. Res., 102, 16 663–16 682.

Brennan, M. J. and S. J. Majumdar, 2011: An examination of model track forecast errors for Hurricane Ike (2008) in the Gulf of Mexico. Wea. Forecasting, In Press.

Smith, R. B., 1993: A hurricane Beta-drift law. *J. Atmos. Sci.*, **50**, 3213-3215.

Torn, R. D. and G. J. Hakim, 2009: Ensemble data assimilation applied to RAINEX observations of Hurricane Katrina (2005). Mon. Wea. Rev., 137, 2817–2829.

−, G. J. Hakim, and C. Snyder, 2006: Boundary conditions for limited-area ensemble Kalman filters. Mon. Wea. Rev., 134, 2490–2502.

Wang, X., 2010: Incorporating ensemble covariance in the Gridpoint Statistical Interpolation (GSI) variational minimization: a mathematical framework. *Mon. Wea. Rev.*, **138**, 2990-2995.

−, and C. H. Bishop, 2003: A comparison of breeding and ensemble transform Kalman filter ensemble forecast schemes. *J. Atmos. Sci.*, **60**, 1140-1158.

−, C. H. Bishop, and Simon J. Julier, 2004: Which is better, an ensemble of positive-negative pairs or a centered spherical simplex ensemble? *Mon. Wea. Rev.*, **132**, 1590-1605.

−, C. Snyder, and T. M. Hamill, 2007a: On the theoretical equivalence of differently proposed ensemble/3D-Var hybrid analysis schemes. *Mon. Wea. Rev.*, **135**, 222-227.

−, T. M. Hamill, J. S. Whitaker and C. H. Bishop, 2007b: A comparison of hybrid ensemble transform Kalman filter-OI and ensemble square-root filter analysis schemes. *Mon. Wea. Rev.*, **135**, 1055-1076.

−, D. Barker, C. Snyder, T. M. Hamill, 2008a: A hybrid ETKF-3DVAR data assimilation scheme for the WRF model. Part I: observing system simulation experiment. *Mon. Wea. Rev.*, **136**, 5116-5131.

−, −, −, −, 2008b: A hybrid ETKF-3DVAR data assimilation scheme for the WRF model. Part II: real observation experiments. *Mon. Wea. Rev.*, **136**, 5132-5147.

−, T. M. Hamill, J. S. Whitaker, C. H. Bishop, 2009: A comparison of the hybrid and EnSRF analysis schemes in the presence of model error due to unresolved scales. *Mon. Wea. Rev.*, **137**, 3219-3232.

Xiao, Q., X. Zhang, C. Davis, J. Tuttle, G. Holland, P. J. Fitzpatrick, 2009a: Experiments of Hurricane Initialization with Airborne Doppler Radar Data for the Advanced Research Hurricane WRF (AHW) Model. *Mon. Wea. Rev*., **137**, 2758-2777.

−, L. Chen, and X. Zhang, 2009b: Evaluations of BDA Scheme Using the Advanced Research WRF (ARW) Model. *Journal of Applied Meteorology and Climatology*, **48**, 680-689.

Zhang, F., Z.Weng, Z.Meng, J. A. Sippel, and C. H. Bishop, 2009: Cloud-resolving hurricane initialization and prediction through assimilation of Dopper radar observations with an ensemble Kalman filter. Mon. Wea. Rev., 137, 2105–2125.

Zou, X. and Q. Xiao, 2000: Studies on the initialization and simulation of a mature hurricane using a variational bogus data assimilation scheme. J. Atmos. Sci., 57, 836–860.

Zupanski, M., 2005: Maximum Likelihood Ensemble Filter: Theoretical Aspects. *Mon. Wea. Rev.,* 133, 1710–1726.

Table Captions

Table 1 The averaged inflation factor (π) and fraction factor (ρ) adaptively determined in the ETKF algorithm in the HYBRID-Ens experiment. The covariance localization scale (S) and the weighting factor $1/\beta_1$ adopted in the HYBRID-Ens experiment are also shown.

Table 2 Assimilated observation types, variables and the corresponding observation errors (numbers below). The left most column denotes the observation types using the WMO (World Meteorological Organization) GTS (Global Telecommunication System) standard (http://www.nws.noaa.gov/tg/tableb1.html). The errors of the wind observations for SOUND, PROFILER and PILOT and the errors of temperature observations for SATEM shown in the table are vertically averaged values. Their corresponding vertical profiles of observation errors are shown in Fig. 4.

Table 3 Starting and ending dates of the data assimilation cycling periods for IKE and GUSTAV 2008.

Figure Captions

Figure 1 Illustration of the hybrid ETKF–3DVAR analysis and ensemble generation cycle for a hypothetical three-member ensemble.

Figure 2 The WRF model domain and the 6-hourly tracks of IKE during 0000 UTC 7 Sep.~1200 UTC 13 Sep. 2008 (black dot) and the GUSTAV during 0000 UTC 27 Aug. ~ 1800 UTC 3 Sep. 2008 (hollow square). The data are obtained from the best track data of the National Hurricane Center.

Figure 3 A snap shot of the observations assimilated at 0000 UTC 7 Sep. 2008: (a) QSCAT; (b) SYNOP; (c) SHIP; (d) METAR; (e) SOUND (including dropsondes); (f) BUOY; (g) PROFILER; (h) PILOT; (i) AIREP; (j) SATEM; (k) SATOB. The naming conventions of these observations follow the WMO standard (www.nws.noaa.gov/tg/tableb1.html).

Figure 4 Observation errors as a function of pressure for the SOUND wind (solid), the PROFILER and PILOT wind (dashed) and the SATEM temperature (dotted) observations.

Figure 5 6-hourly analyzed tracks by the HYBRID-Ens, 3DVAR and HYBRID-Static for IKE during the data assimilation period. The best track data is also shown as a reference.

Figure 6 6-hourly absolute errors of the analyzed tracks verified against the best track data for the HYBRID-Ens, 3DVAR and HYBRID-Static for IKE during the data assimilation period.

Figure 7 Root mean square errors of the track forecasts by the HYBRID-Static (dotted), HYBRID-Ens (solid) and 3DVAR (dashed) up to the 72-hour lead time for forecasts initialized every 12 hours during the assimilation period for IKE.

Figure 8 Track forecasts initialized by the analyses at 0000 UTC Sep. 9 2008 for the HYBRID-Static, HYBRID-Ens and 3DVAR for IKE. The best track data and the WRF forecasts initialized by the GFS analysis (denoted as GFS) are shown as references.

Figure 9 500 hPa geopotential height (in meters) for the HYBRID-Ens analysis (a) and the 3DVAR analysis (b) valid at 0000 UTC Sep. 9 2008 for IKE.

Figure 10 48-hour forecasts of 500 hPa geopotential height (in meters) initialized at 0000UTC Sep. 9 2008 from the analyses generated by the HYBRID-Ens (a) and by the 3DVAR (b).

Figure 11 East-West vertical cross section of the wind speed (in ms^{-1}) for the analyses at 0000UTC Sep. 9 2008. (a) is for the HYBRID-Ens analysis and (b) is for the 3DVAR analysis. The cross section cuts cross the maximum relative vorticity at 500 hPa.

Figure 12 The color shades in (a) and (b) show the 500 hPa geopotential height increments by the 3DVAR and the HYBRID-Ens respectively. The color shades in (c) show the 500 hPa geopotential height background ensemble spread for the HYBRID-Ens. They are valid at 0000 UTC Sep. 8 2008 for IKE. The black contours in (a), (b) and (c) are the corresponding background 500 hPa geopotential height fields valid at 0000 UTC Sep. 8 2008.

Figure 13 The 6-hourly analyzed tracks by the HYBRID-Ens, 3DVAR and HYBRID-Static for GUSTAV during the data assimilation period. The best track data is also shown as a reference.

Figure 14 The 6-hourly absolute errors of the analyzed tracks verified against the best track data by the HYBRID-Ens, 3DVAR and HYBRID-Static for GUSTAV during the data assimilation period.

Figure 15 The root mean square errors of the track forecasts by the HYBRID-Static (dotted), HYBRID-Ens (solid) and 3DVAR (dashed) up to 72 hour lead time for forecasts initialized every 12 hours during the assimilation period for GUSTAV.

Figure 16 The 500 hPa geopotential height (in meters) for the HYBRID-Ens analysis (a) and the 3DVAR analysis (b) valid at 0000UTC Aug. 29 2008 for GUSTAV.

Figure 17 Locations of dropsondes in the vicinity of Gustav during 0000 UTC-1800 UTC Aug. 29: the filled black circle denotes the dropsonde around 0009 UTC Aug. 29 and the upward triangles denote the dropsondes around 1800 UTC Aug. 29. Also shown are the Gustav locations in the background forecast of the 3DVAR valid at 0009 UTC Aug. 29 (empty circle) and at 1800 UTC Aug. 29 (downward triangle).

Figure 18 The 500 hPa increments (color shades) by the 3DVAR (a) and the HYBRID-Ens (b) valid at 0000 UTC Aug. 31 2008. The black contours are the corresponding background forecasts of 500 hPa geopotential height (in meters).

Table 1 The averaged inflation factor (π) and fraction factor (ρ) adaptively determined in the ETKF algorithm in the HYBRID-Ens experiment. The covariance localization scale (S) and the weighting factor $1/\beta_1$ adopted in the HYBRID-Ens experiment are also shown.

	π	ρ	S	$1/\beta_1$
IKE	6.70	39.96%	1500 km	0
GUSTAV	7.22	38.94%	1500 km	0

Table 2 Assimilated observation types, variables and the corresponding observation errors (numbers below). The left most column denotes the observation types using the WMO (World Meteorological Organization) GTS (Global Telecommunication System) standard (http://www.nws.noaa.gov/tg/tableb1.html). The errors of the wind observations for SOUND, PROFILER and PILOT and the errors of temperature observations for SATEM shown in the table are vertically averaged values. Their corresponding vertical profiles of observation errors are shown in Fig. 4.

	Wind (m/s)	Temperature (K)	Pressure (hPa)	Relative Humidity (%)
QSCAT	2.5	--	--	--
SYNOP	1.1	2	1	10
SHIP	1.1	2	1.6	10
METAR	1.1	2	1	10
SOUND	2.1 (Fig. 4)	1	--	10.3
BUOY	1.4	2	1	10
PROFILER	2.6 (Fig. 4)	--	--	--
PILOT	2.6 (Fig. 4)	--	--	--
AIREP	3.6	1	--	--
SATEM	--	2.3 (Fig. 4)	--	--
SATOB	4.5 above 800 hPa 2.5 below 800 hPa	--	--	--

Table 3 Starting and ending dates of the data assimilation cycling periods for IKE and GUSTAV 2008.

Cycling start date	Cycling end date	Storms
0000 UTC 7 Sep. 2008	1200 UTC 13 Sep. 2008	IKE
0000 UTC 27 Aug. 2008	1800 UTC 3 Sep. 2008	GUSTAV

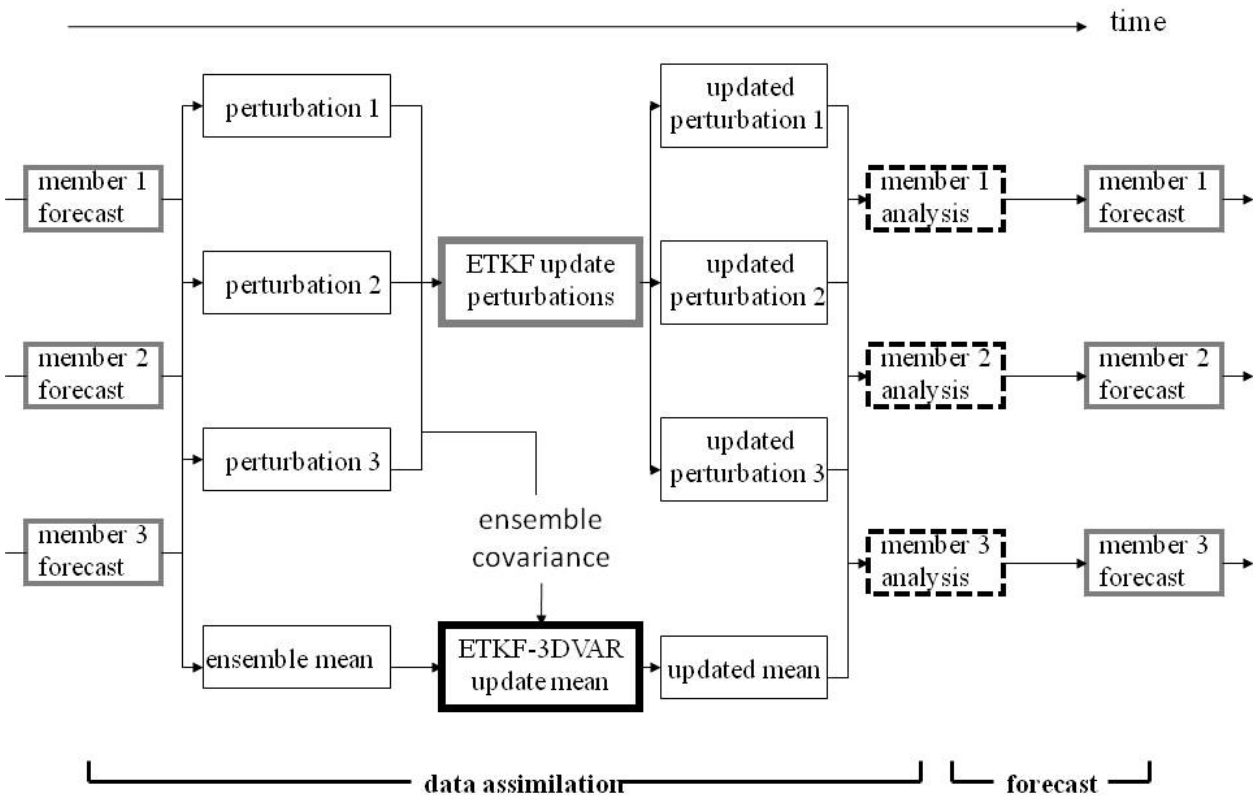

Figure 1 Illustration of the hybrid ETKF–3DVAR analysis and ensemble generation cycle for a hypothetical three-member ensemble.

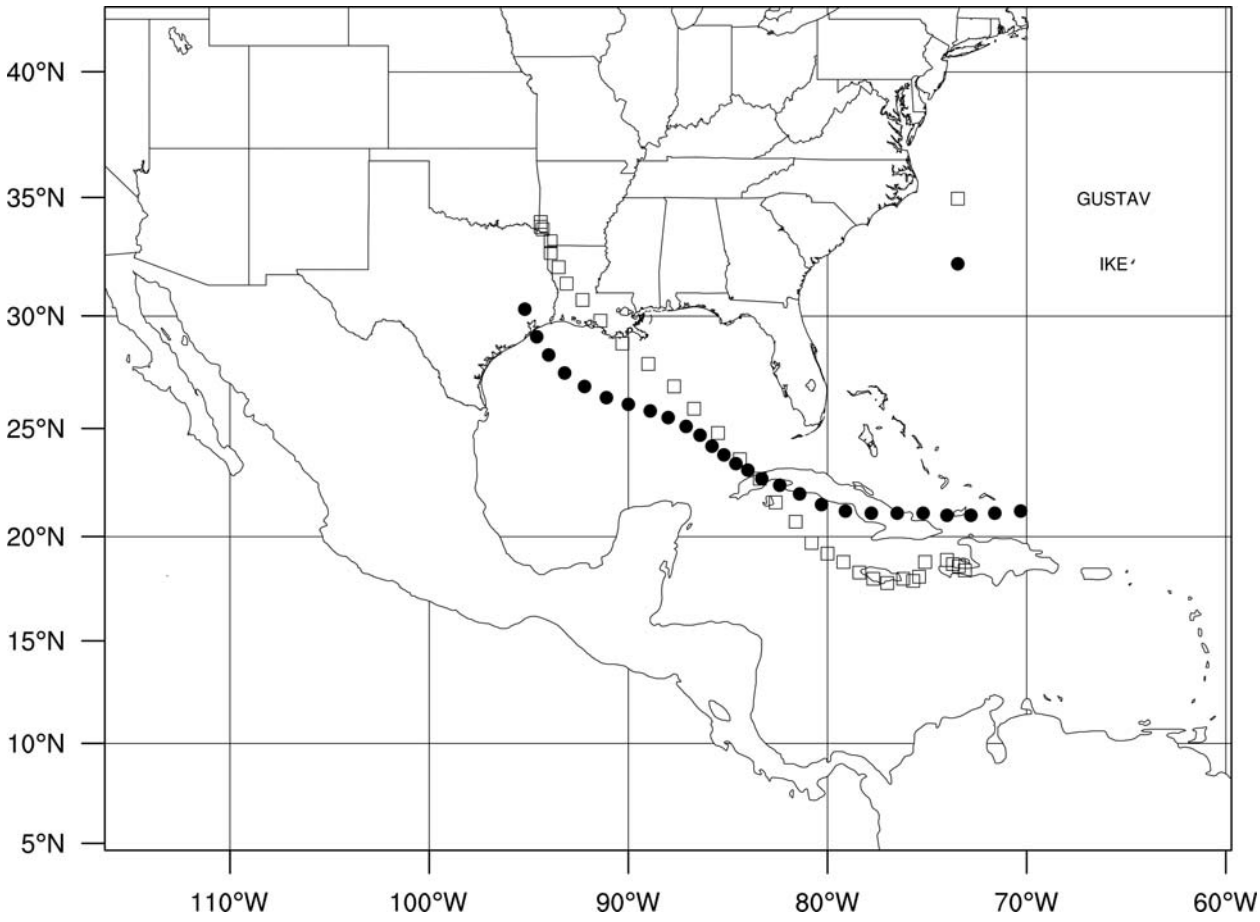

Figure 2 The WRF model domain and the 6-hourly tracks of IKE during 0000 UTC 7 Sep.~1200 UTC 13 Sep. 2008 (black dot) and the GUSTAV during 0000 UTC 27 Aug. ~ 1800 UTC 3 Sep. 2008 (hollow square). The data are obtained from the best track data of the National Hurricane Center.

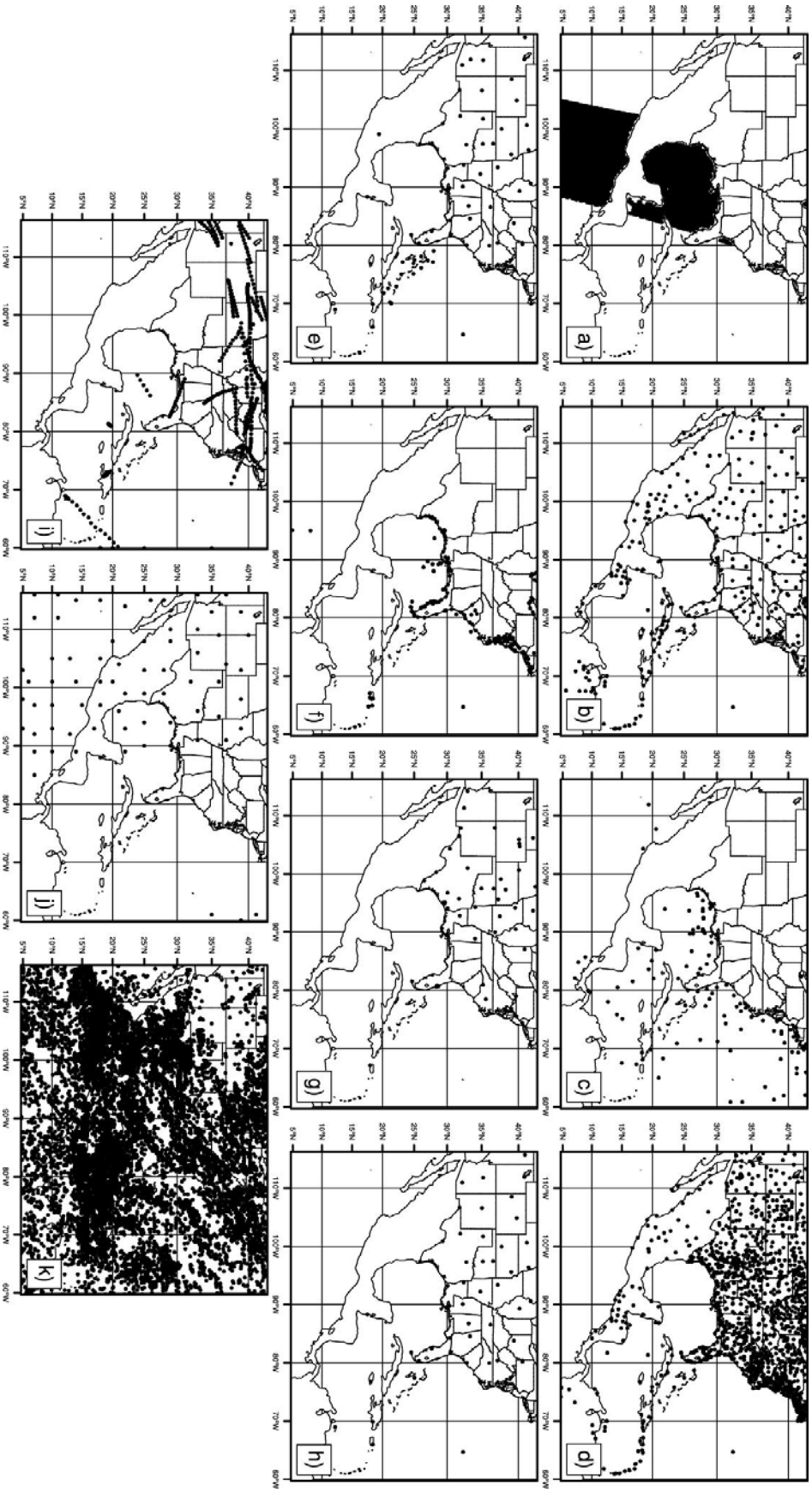

1

Figure 3 A snap shot of the observations assimilated at 0000 UTC 7 Sep. 2008: (a) QSCAT; (b) SYNOP; (c) SHIP; (d) METAR; (e) SOUND (including dropsondes); (f) BUOY; (g) PROFILER; (h) PILOT; (i) AIREP; (j) SATEM; (k) SATOB. The naming conventions of these observations follow the WMO standard (www.nws.noaa.gov/tg/tableb1.html).

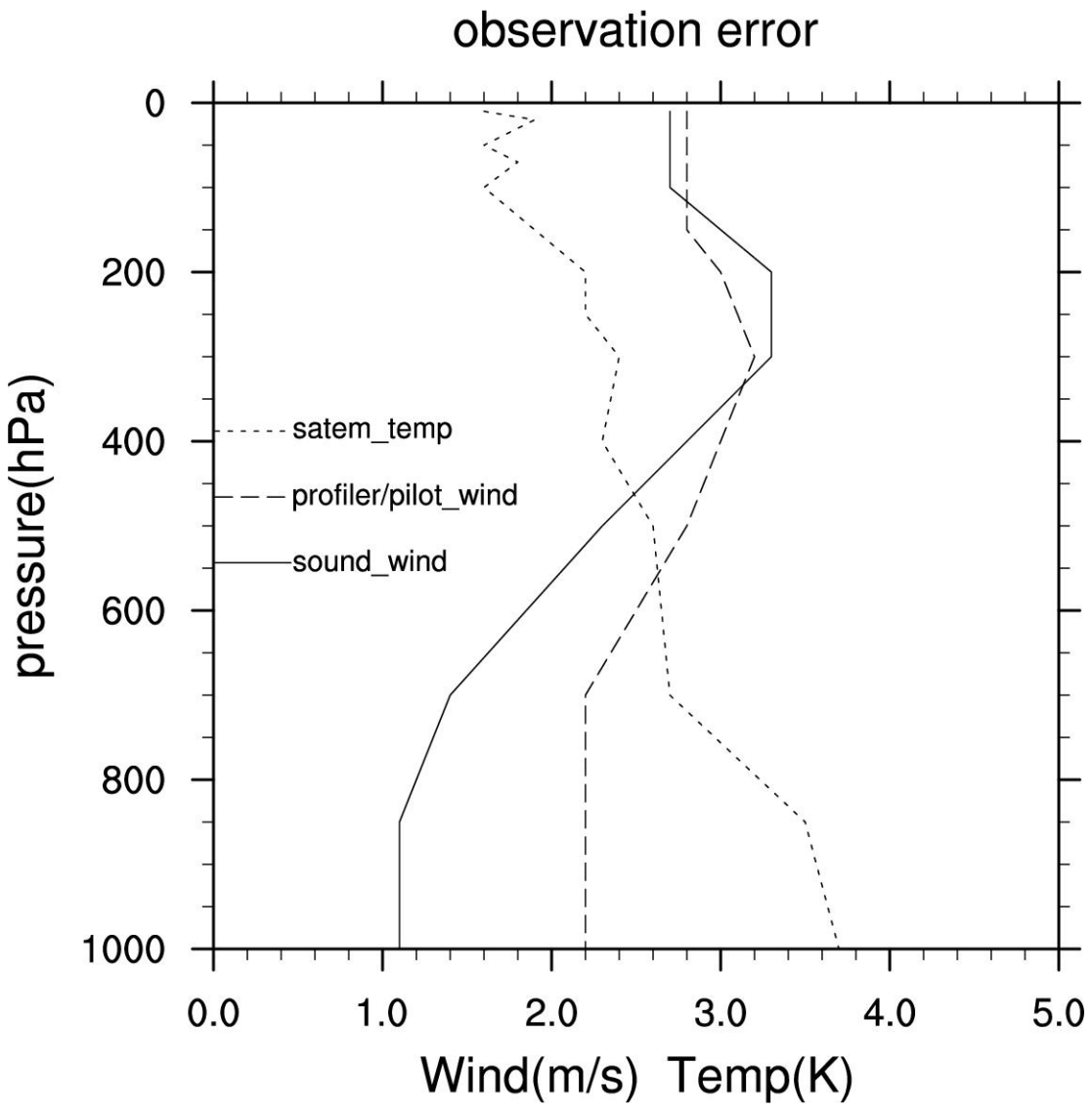

Figure 4 Observation errors as a function of pressure for the SOUND wind (solid), the PROFILER and PILOT wind (dashed) and the SATEM temperature (dotted) observations.

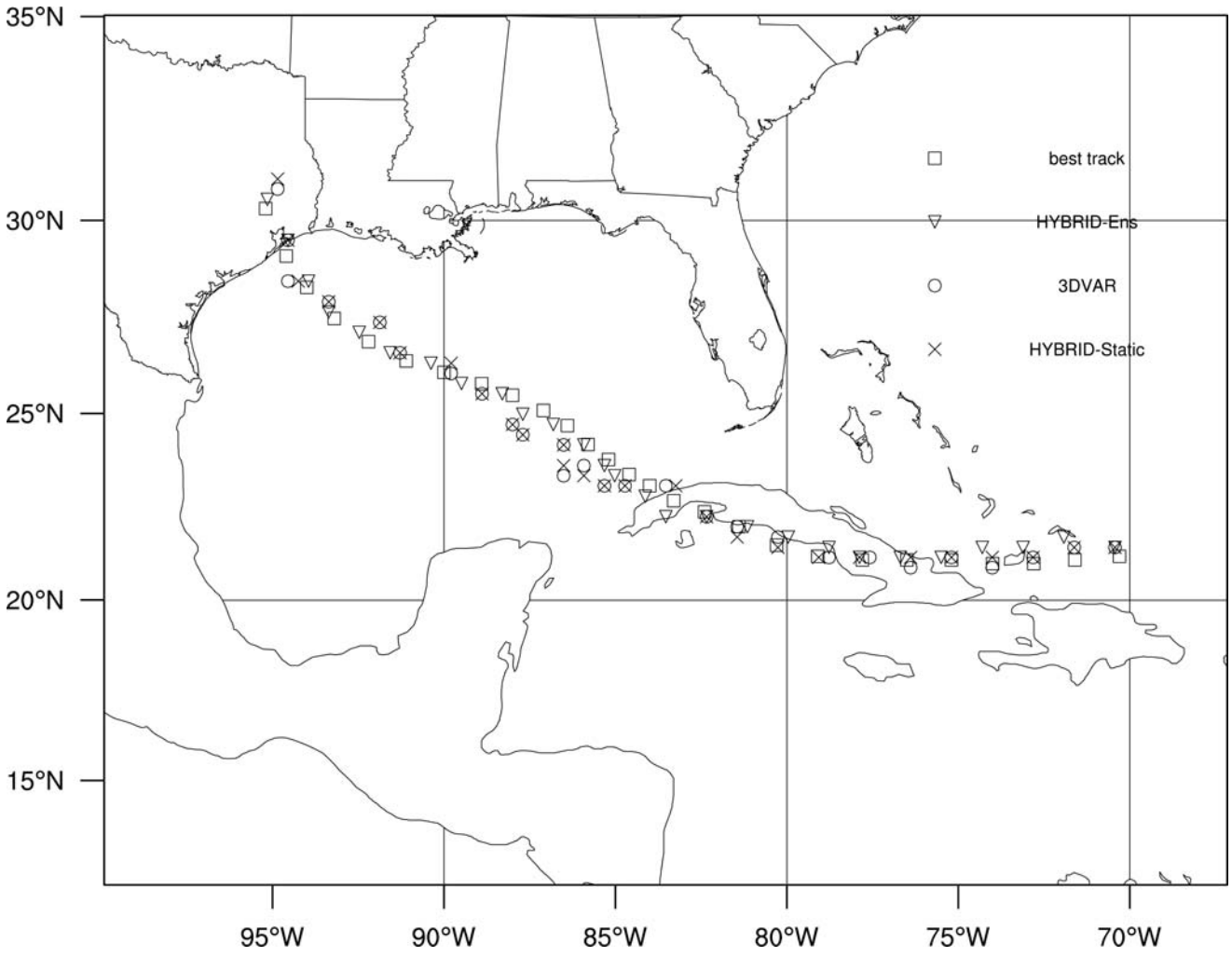

Figure 5 6-hourly analyzed tracks by the HYBRID-Ens, 3DVAR and HYBRID-Static for IKE during the data assimilation period. The best track data is also shown as a reference.

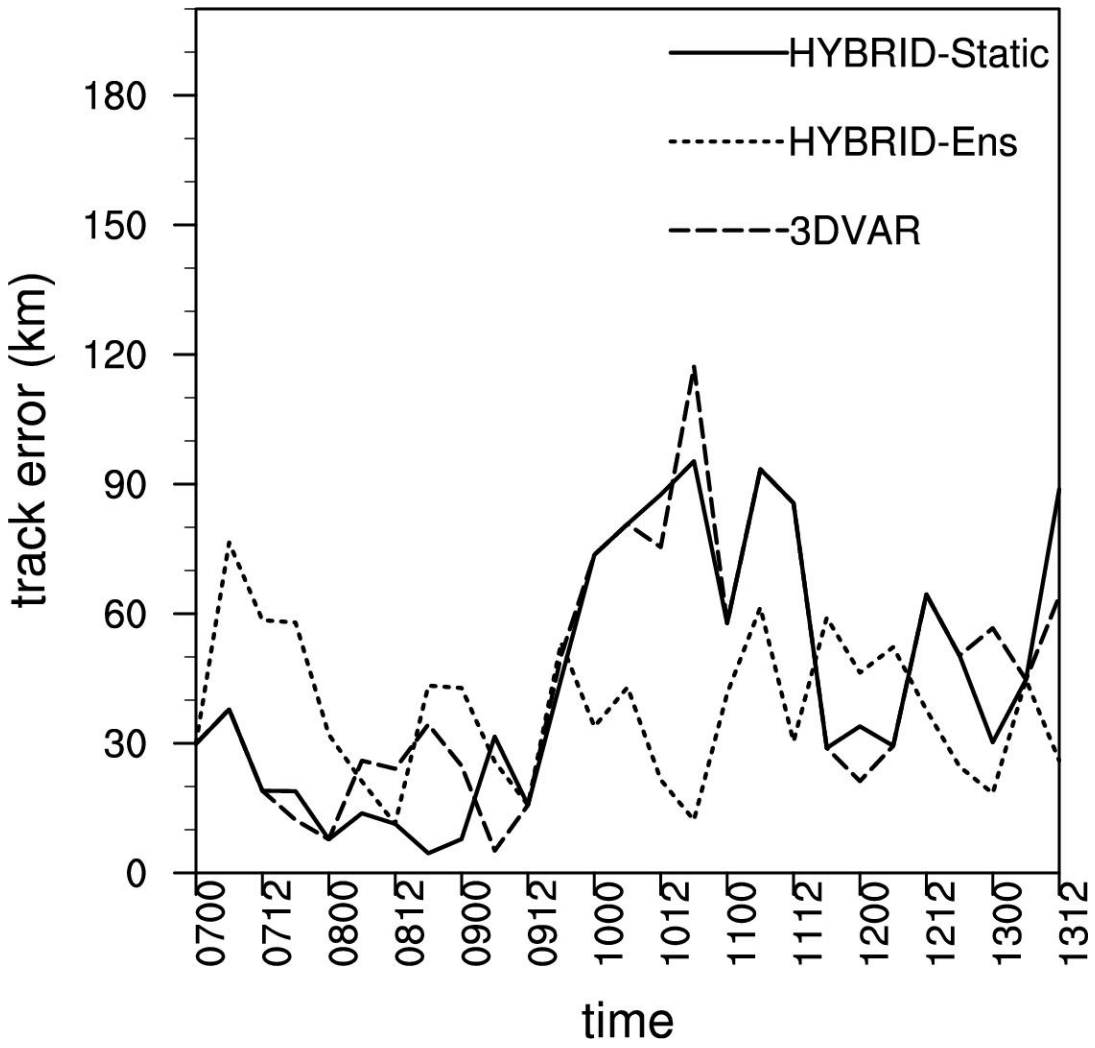

Figure 6 6-hourly absolute errors of the analyzed tracks verified against the best track data for the HYBRID-Ens, 3DVAR and HYBRID-Static for IKE during the data assimilation period.

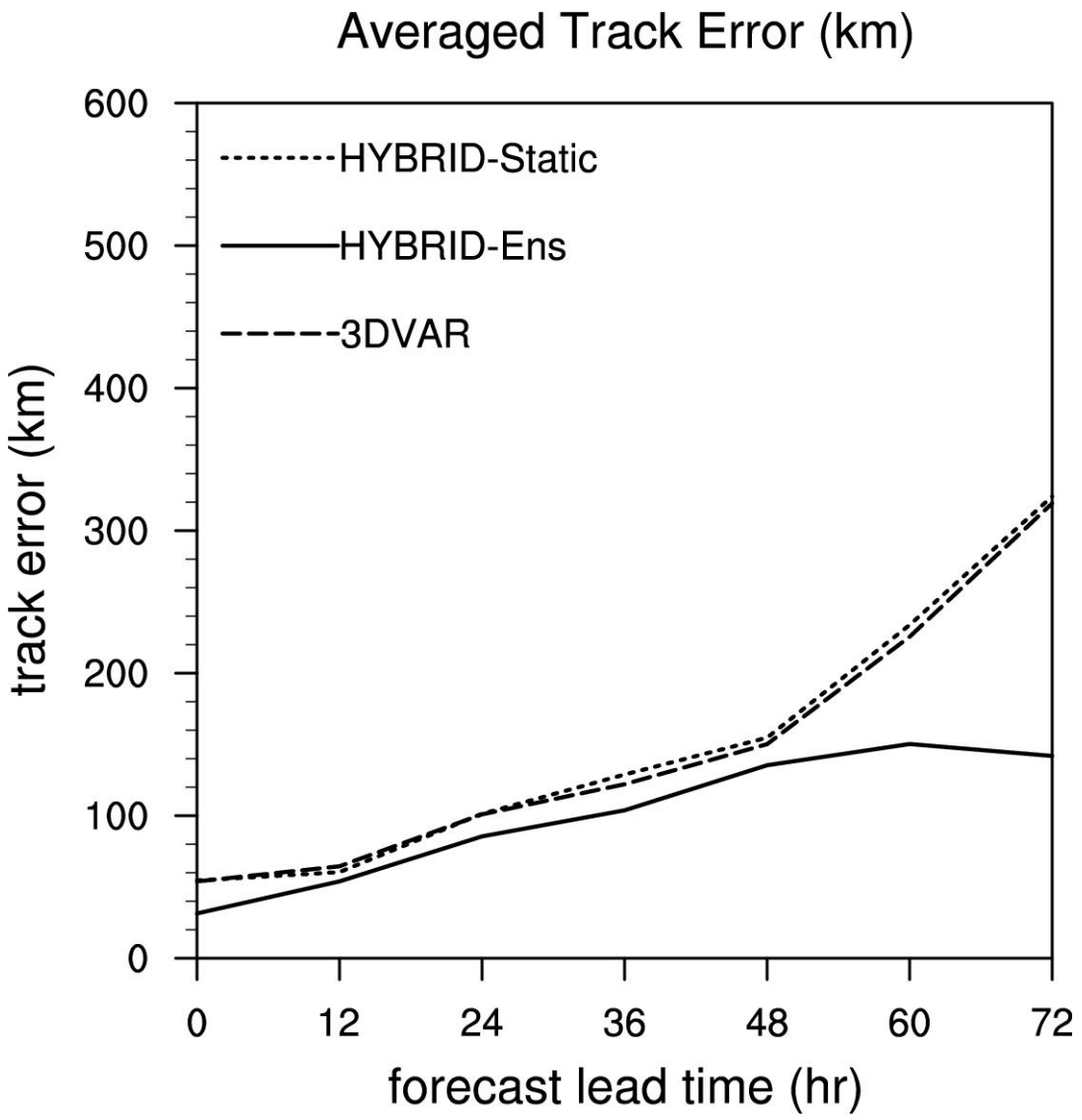

Figure 7 Root mean square errors of the track forecasts by the HYBRID-Static (dotted), HYBRID-Ens (solid) and 3DVAR (dashed) up to the 72-hour lead time for forecasts initialized every 12 hours during the assimilation period for IKE.

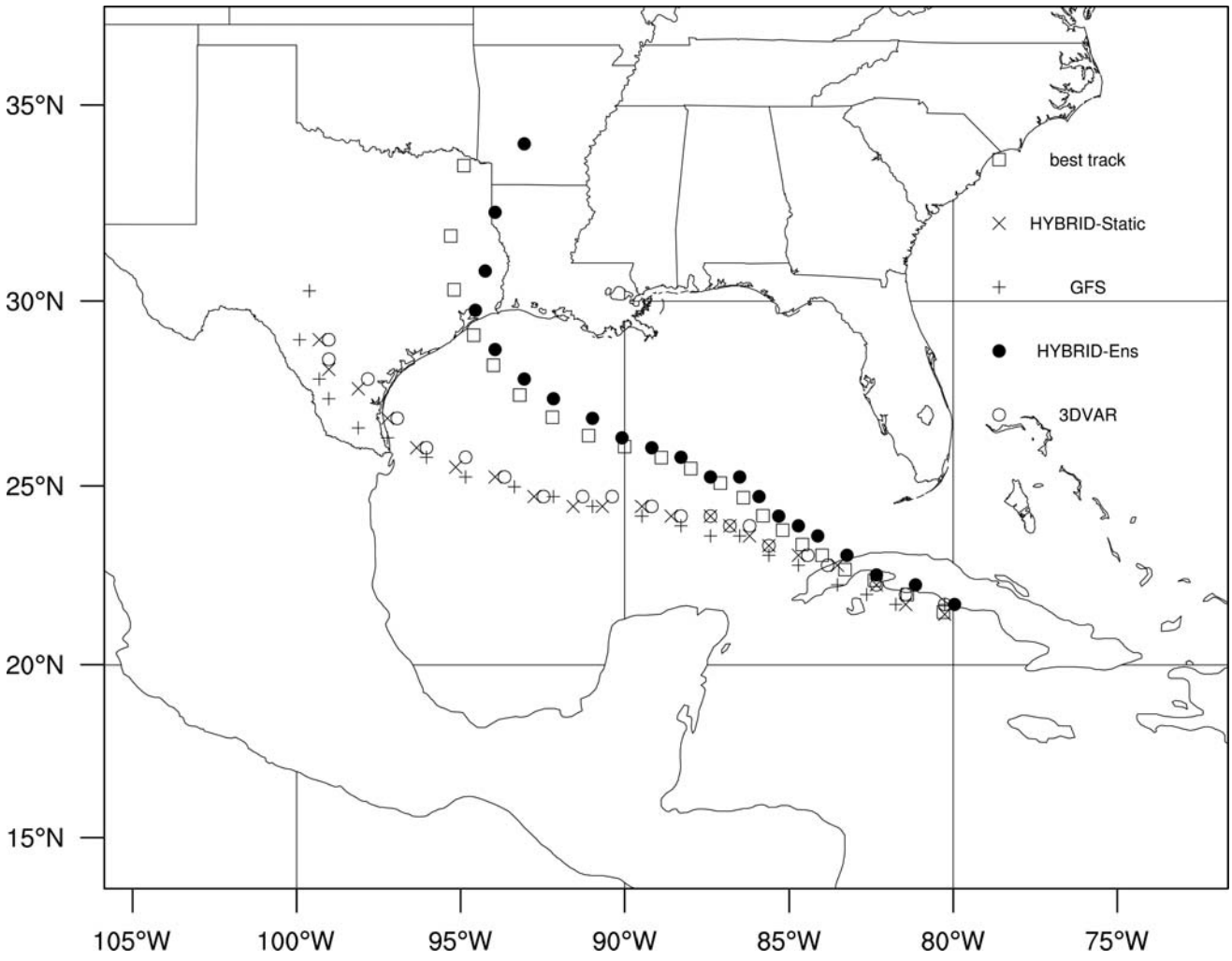

Figure 8 Track forecasts initialized by the analyses at 0000 UTC Sep. 9 2008 for the HYBRID-Static, HYBRID-Ens and 3DVAR for IKE. The best track data and the WRF forecasts initialized by the GFS analysis (denoted as GFS) are shown as references.

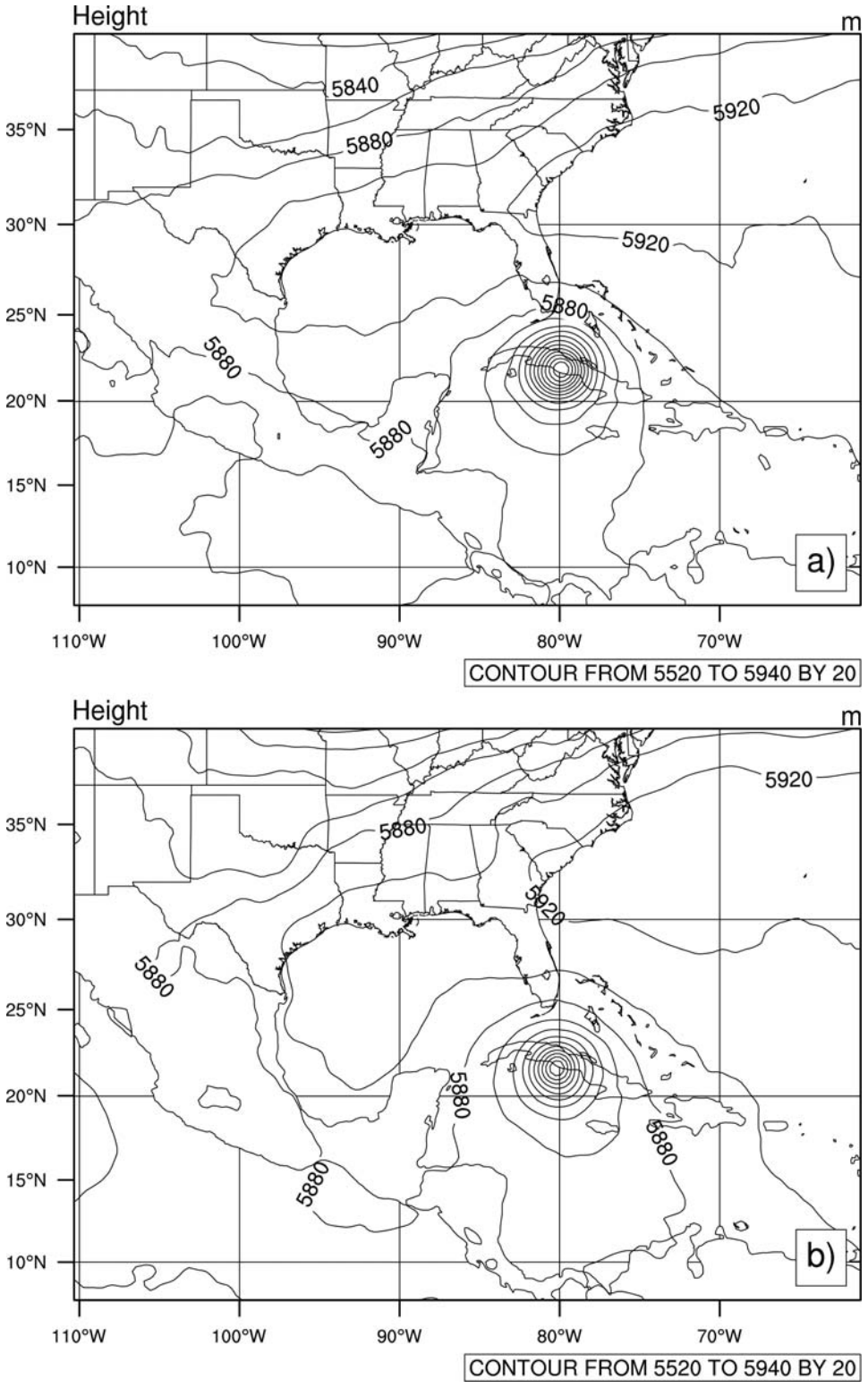

Figure 9 500 hPa geopotential height (in meters) for the HYBRID-Ens analysis (a) and the 3DVAR analysis (b) valid at 0000 UTC Sep. 9 2008 for IKE.

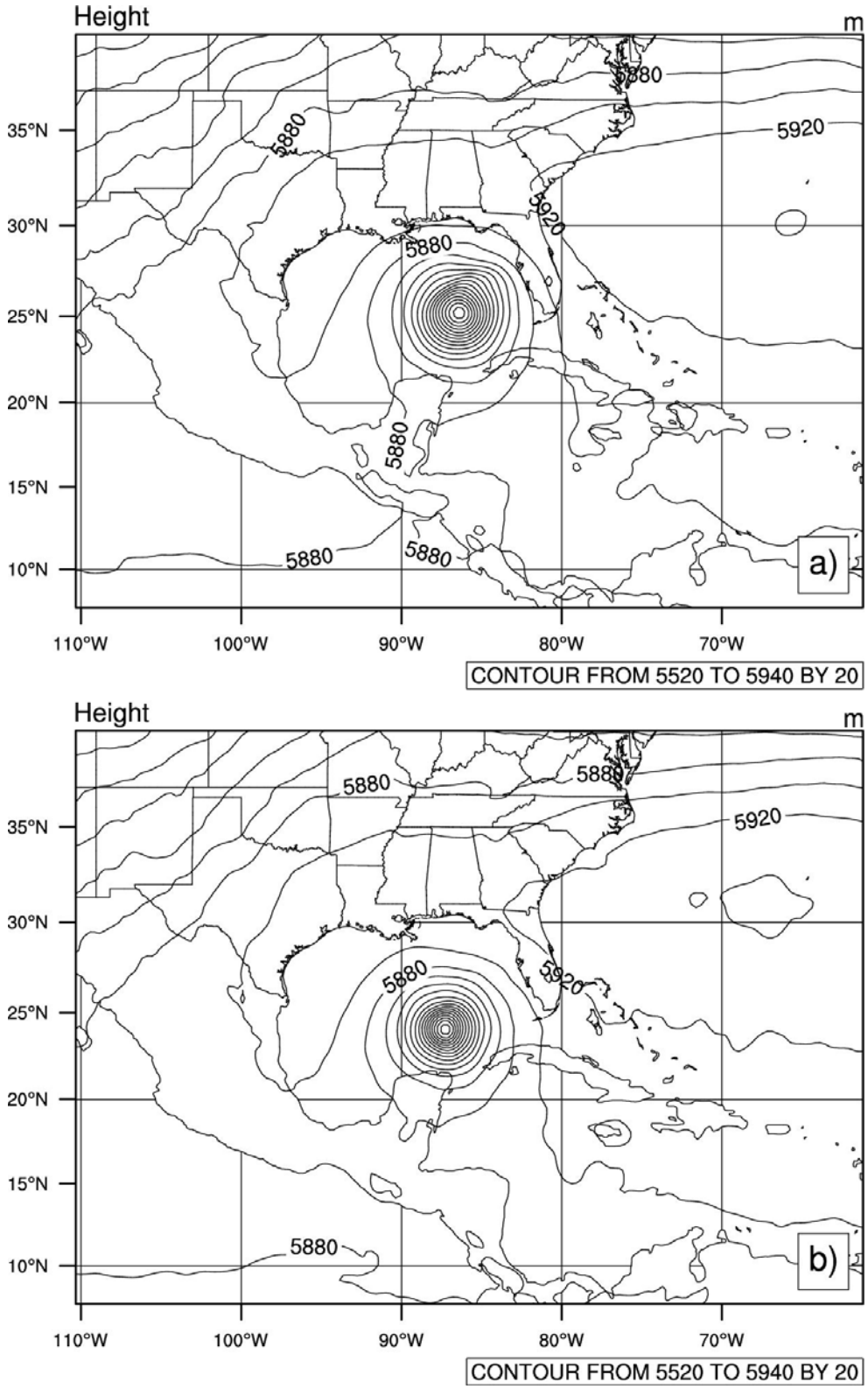

Figure 10 48-hour forecasts of 500 hPa geopotential height (in meters) initialized at 0000UTC Sep. 9 2008 from the analyses generated by the HYBRID-Ens (a) and by the 3DVAR (b).

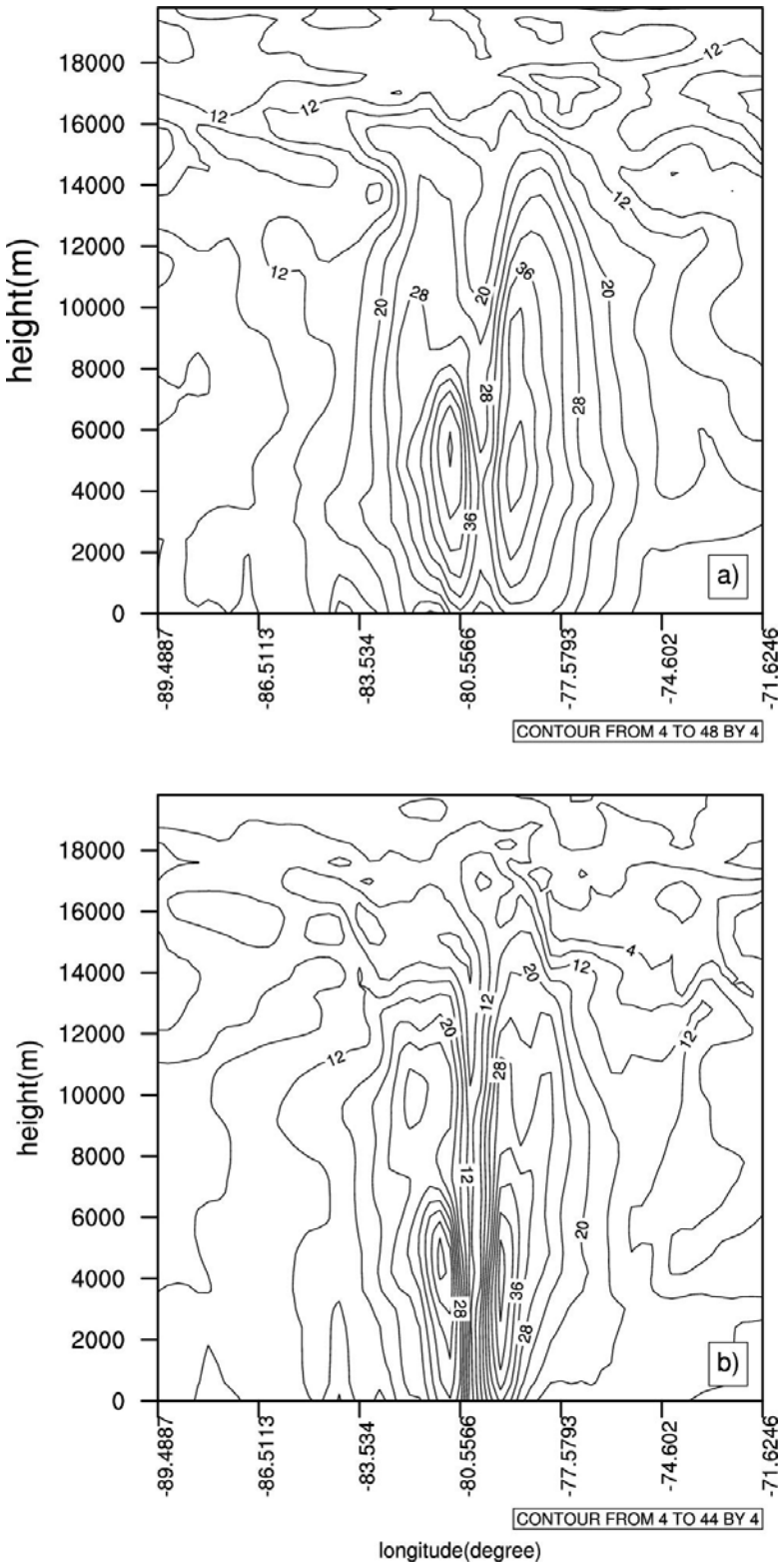

Figure 11 East-West vertical cross section of the wind speed (in ms^{-1}) for the analyses at 0000UTC Sep. 9 2008. (a) is for the HYBRID-Ens analysis and (b) is for the 3DVAR analysis. The cross section cuts cross the maximum relative vorticity at 500 hPa.

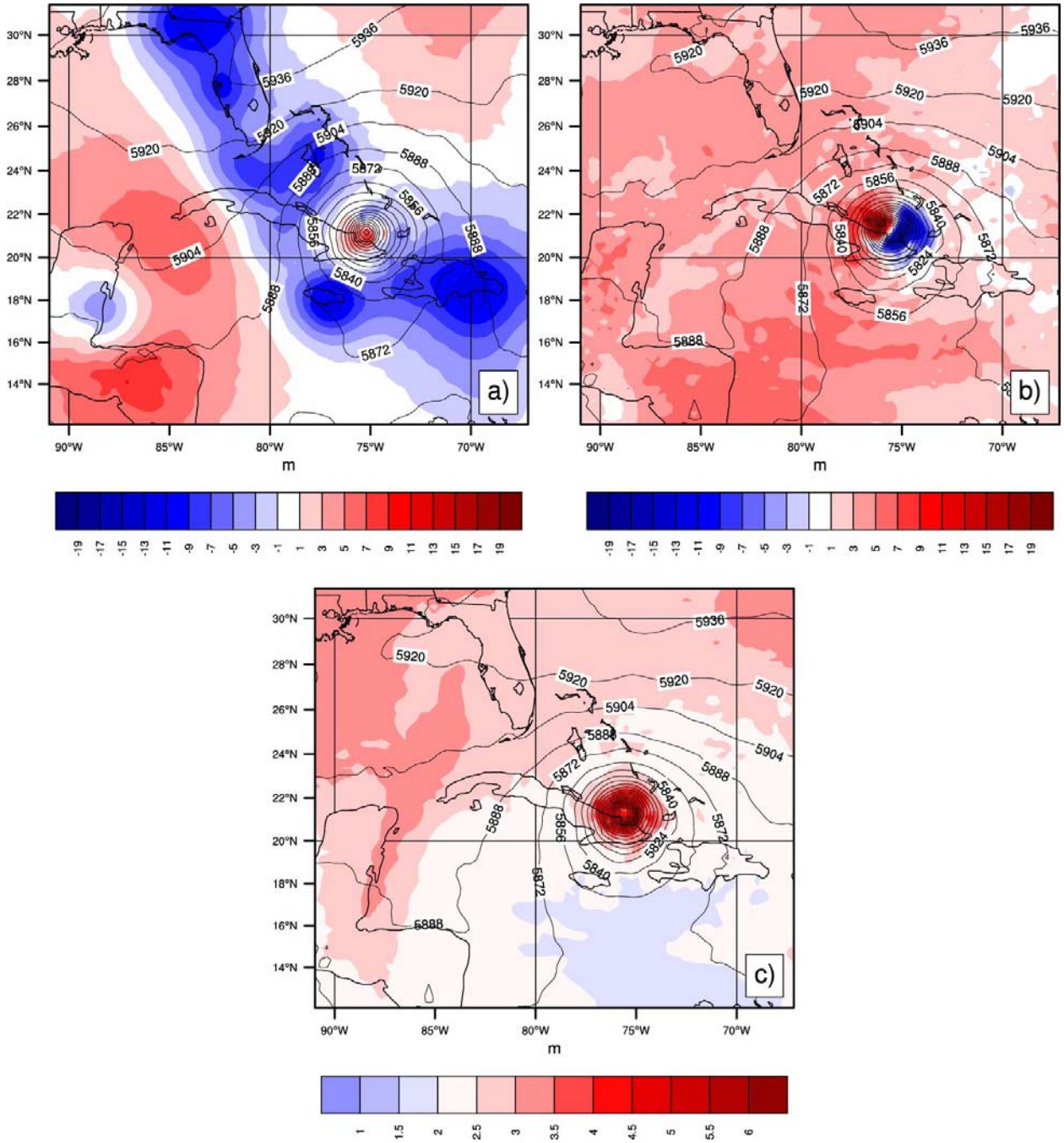

Figure 12 The color shades in (a) and (b) show the 500 hPa geopotential height increments by the 3DVAR and the HYBRID-Ens respectively. The color shades in (c) show the 500 hPa height background ensemble spread for the HYBRID-Ens. They are valid at 0000 UTC Sep. 8 2008 for IKE. The black contours in (a), (b) and (c) are the corresponding background 500 hPa geopotential height fields valid at 0000 UTC Sep. 8 2008.

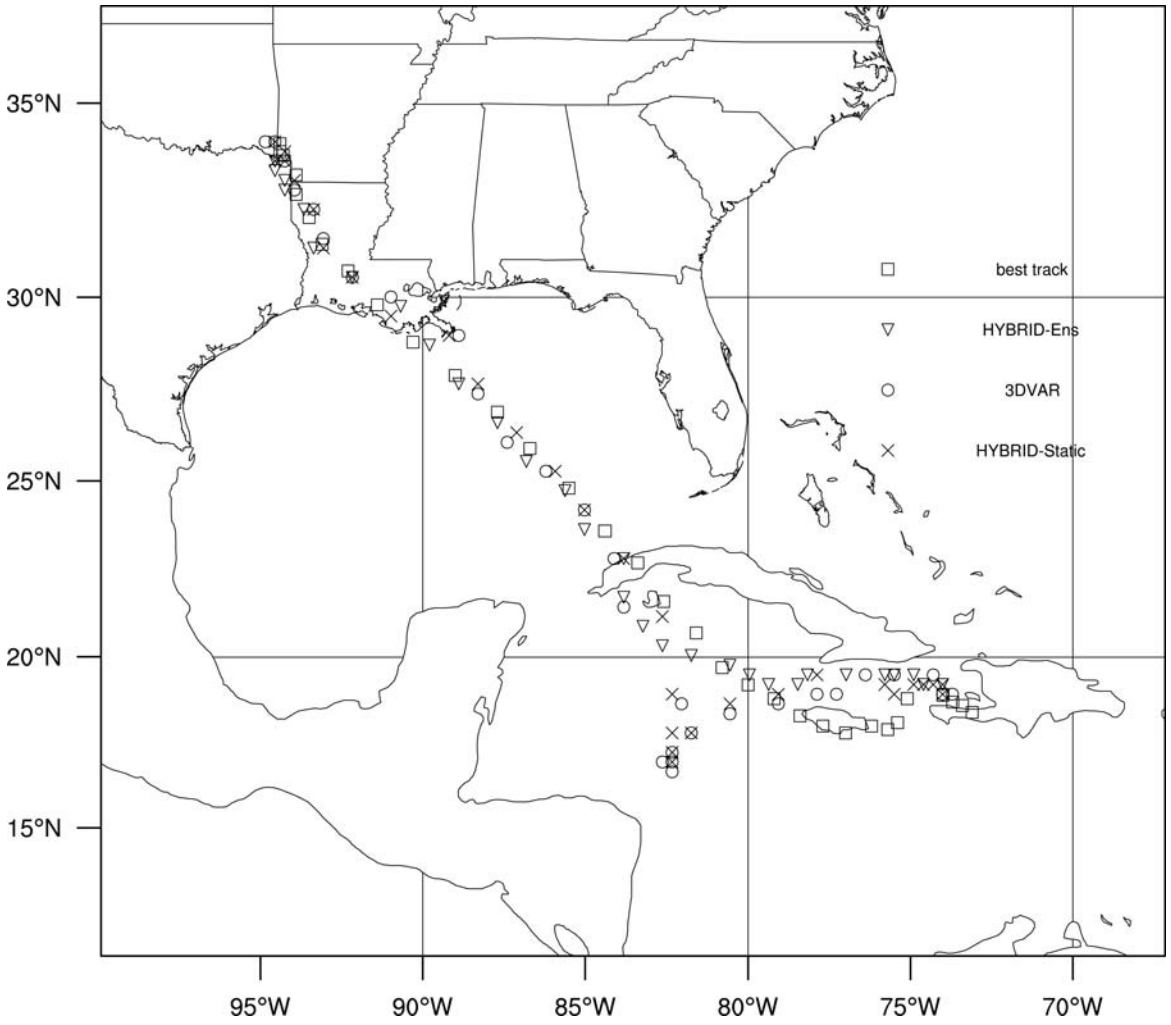

Figure 13 The 6-hourly analyzed tracks by the HYBRID-Ens, 3DVAR and HYBRID-Static for GUSTAV during the data assimilation period. The best track data is also shown as a reference.

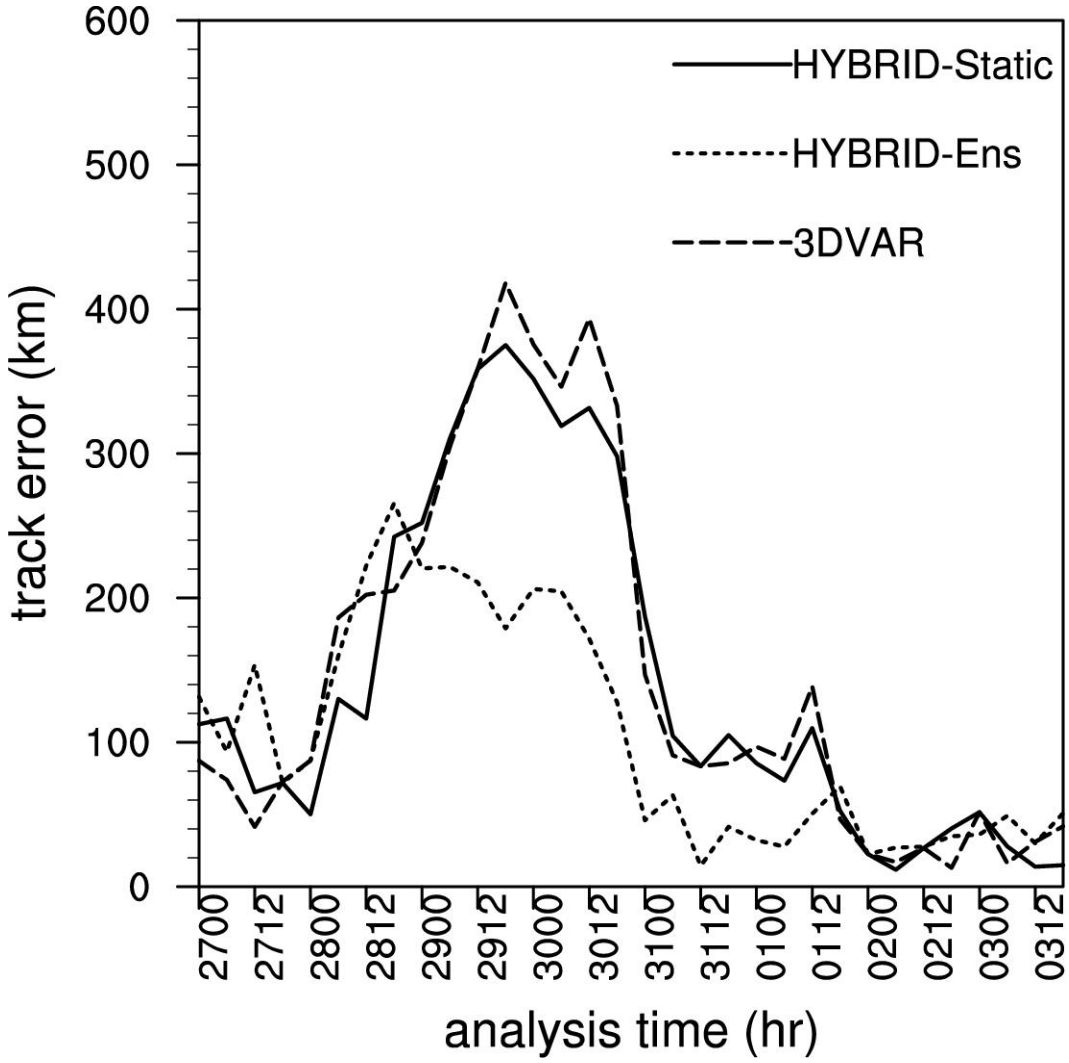

Figure 14 The 6-hourly absolute errors of the analyzed tracks verified against the best track data by the HYBRID-Ens, 3DVAR and HYBRID-Static for GUSTAV during the data assimilation period.

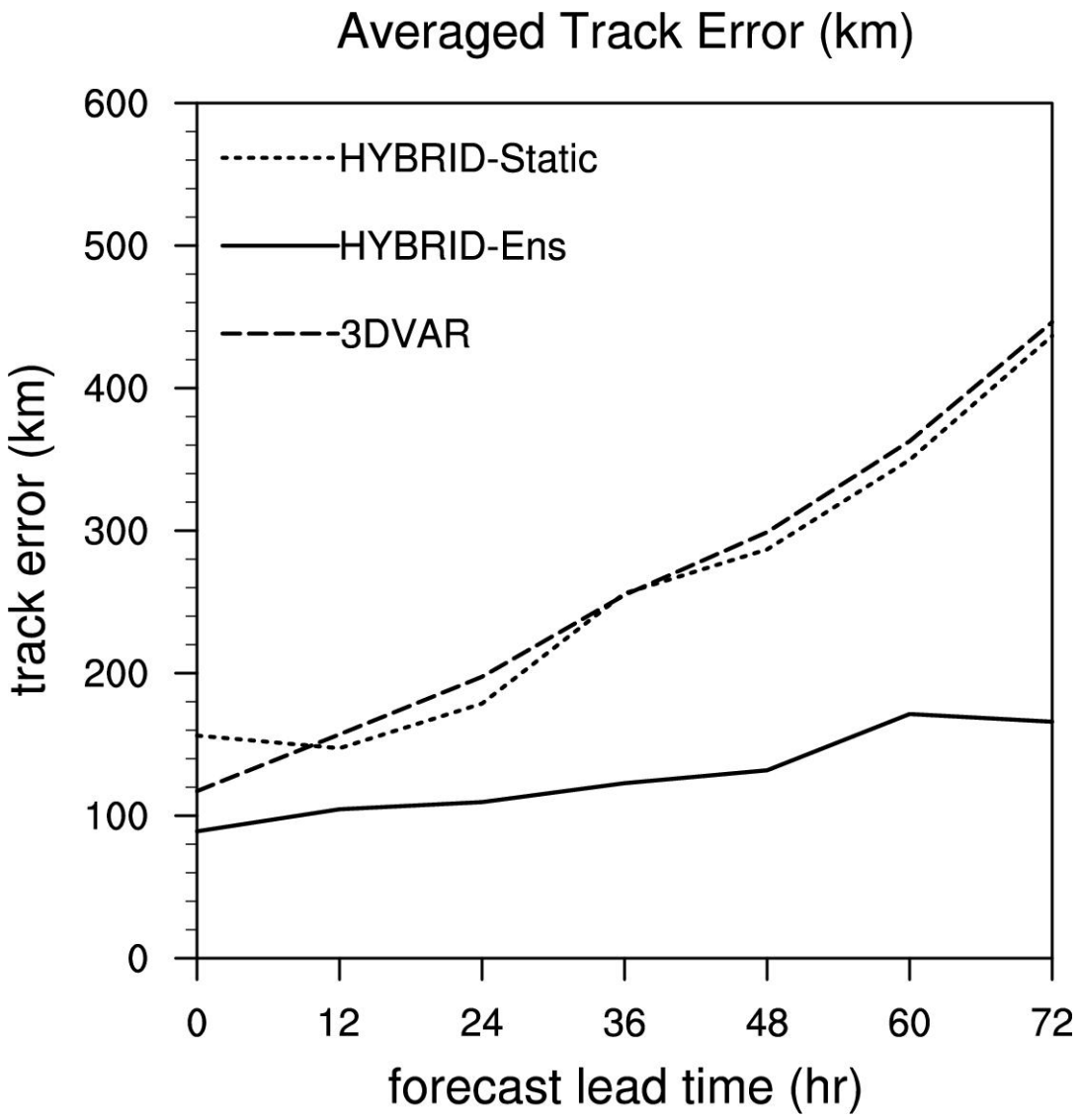

Figure 15 The root mean square errors of the track forecasts by the HYBRID-Static (dotted), HYBRID-Ens (solid) and 3DVAR (dashed) up to 72 hour lead time for forecasts initialized every 12 hours during the assimilation period for GUSTAV.

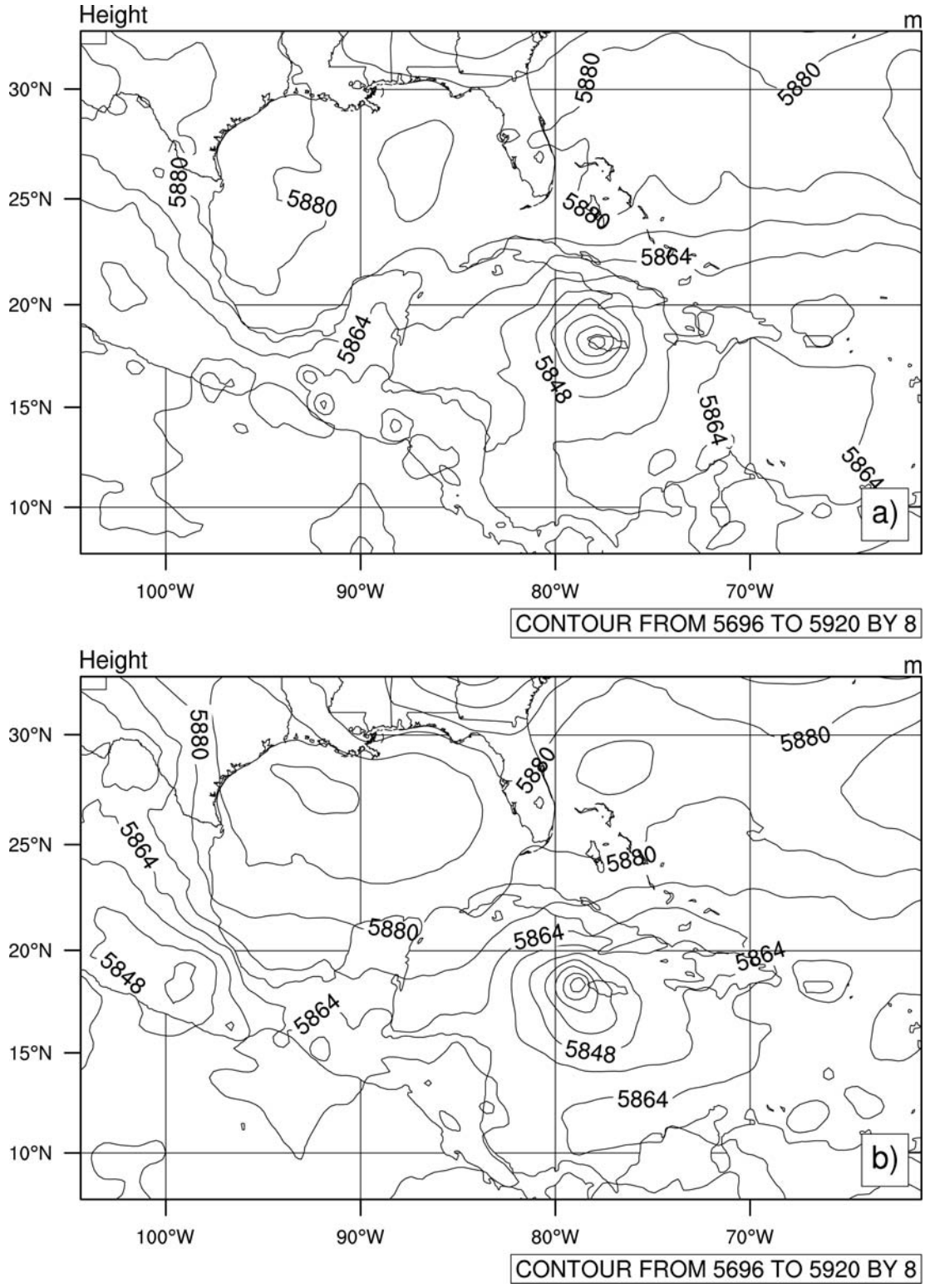

Figure 16 The 500 hPa geopotential height (in meters) for the HYBRID-Ens analysis (a) and the 3DVAR analysis (b) valid at 0000UTC Aug. 29 2008 for GUSTAV.

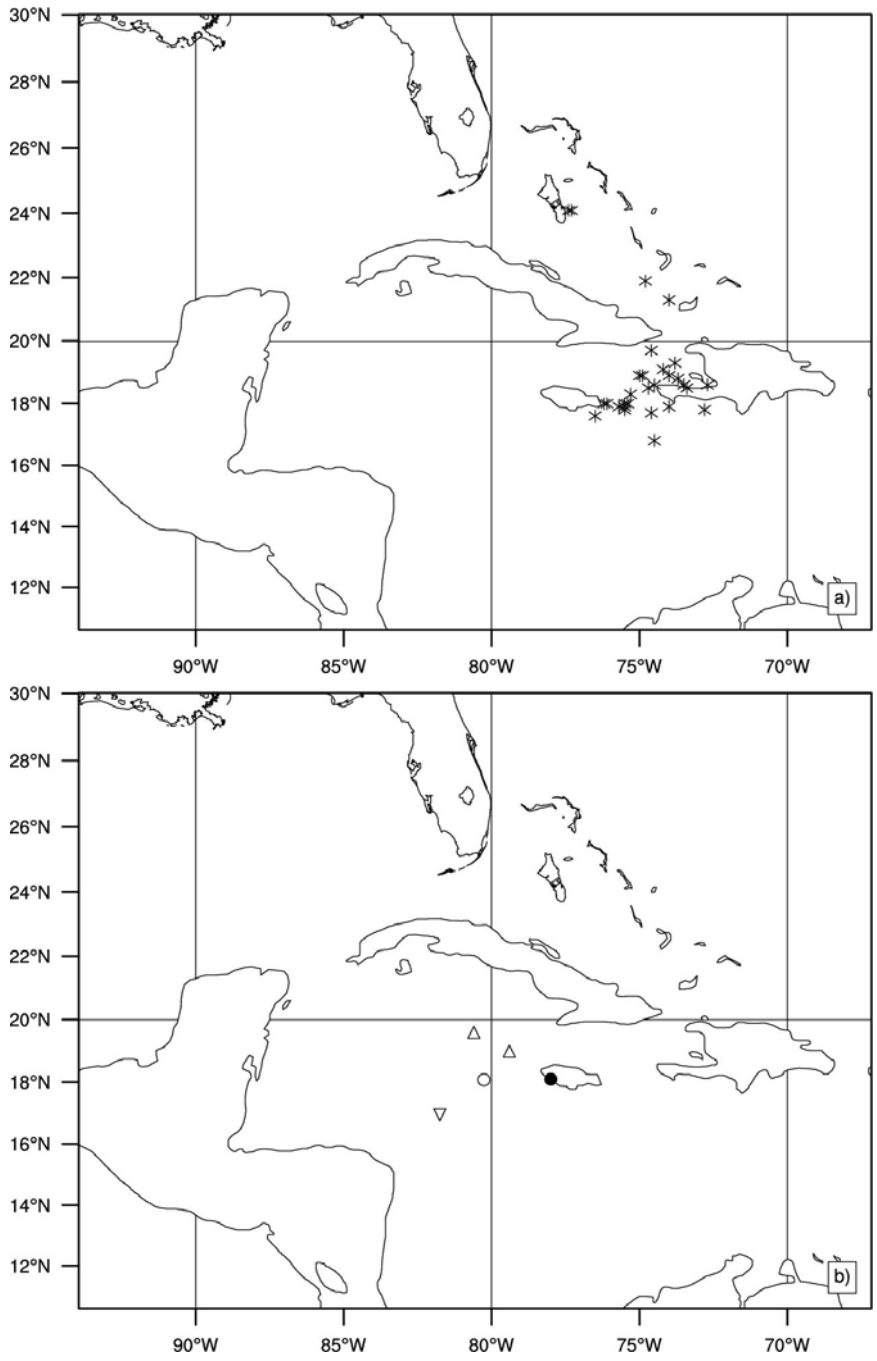

Figure 17 Locations of dropsondes in the vicinity of Gustav during 0000 UTC-1800 UTC Aug. 29: the filled black circle denotes the dropsonde around 0009 UTC Aug. 29 and the upward triangles denote the dropsondes around 1800 UTC Aug. 29. Also shown are the Gustav locations in the background forecast of the 3DVAR valid at 0009 UTC Aug. 29 (empty circle) and at 1800 UTC Aug. 29 (downward triangle).

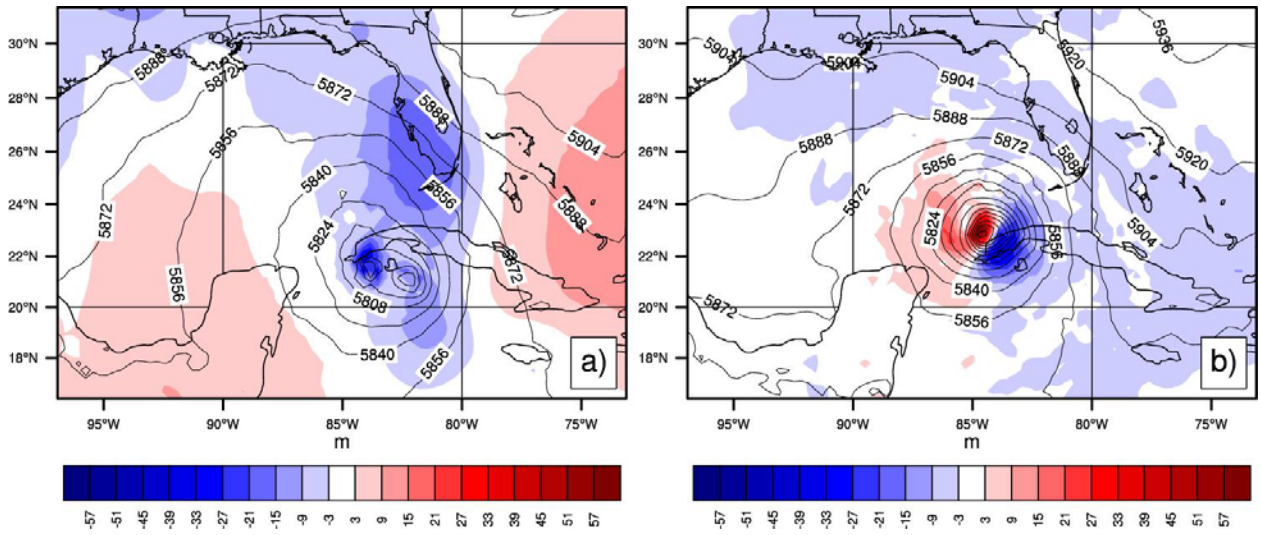

Figure 18 The 500 hPa increments (color shades) by the 3DVAR (a) and the HYBRID-Ens (b) valid at 0000 UTC Aug. 31 2008. The black contours are the corresponding background forecasts of 500 hPa geopotential height (in meters).